The Astrophysical Journal, 711:711–730, 2010 March 10 doi:10.1088/0004-637X/711/2/711

QUANTIFYING SPECTRAL FEATURES OF TYPE Ia SUPERNOVAE

A. Wagers[1], L. Wang[1], and S. Asztalos[2]
[1] Department of Physics, Texas A&M, College Station, TX 77843, USA
[2] X-ray Instrumentation Associates, LLC, Hayward, CA 94551, USA; steve@xia.com
Received 2009 June 25; accepted 2010 January 18; published 2010 February 18

ABSTRACT

We introduce a new technique to quantify highly structured spectra for which the definition of continua or spectral features in the observed flux spectra is difficult. The method employs wavelet transformations to decompose the observed spectra into different scales. A procedure is formulated to define the strength of spectral features so that the measured spectral indices are independent of the flux levels and are insensitive to the definition of continuum and also to reddening. This technique is applied to Type Ia supernovae (SNe) spectra, where correlations are revealed between luminosity and spectral features. The current technique may allow for luminosity corrections based on spectral features in the use of Type Ia SNe as cosmological probe.

Key words: dark energy – supernovae: general

Online-only material: color figures

1. INTRODUCTION

A major difficulty in analyzing spectroscopic data with highly blended atomic lines is to quantify the strength of certain spectral features. These spectral features are superimposed on a continuum so line blending can make it difficult to reliably define the continuum level. In the case of supernova (SN) spectra, the pre-nebular phase spectra typically show P-Cygni profiles, with both emission and absorption components, whereas the nebular phase spectra are dominated by broad overlapping emission lines. The spectral features are therefore of various widths and strengths, and neighboring features are heavily blended. Further, the data typically contain observational noise, flux calibrations errors, and uncertainties in the amount of dust extinction. The noise makes the definition of a continuum very uncertain and, accordingly, the calculation of equivalent width (EW) unreliable. In many observations, in particular, those at high redshift, the observed SN spectra are heavily contaminated by the host galaxy, further affecting the definition of line depth.

For Type Ia SNe, it is known that certain spectral line ratios such as the Si II 5972/Si II 6355, and the Ca II H&K lines are sensitive to the intrinsic brightness of the SN (Nugent et al. 1995). The measurement of the line strength is, however, not trivial. For instance, to measure the Si II 5972/Si II 6355, and the Ca II ratio, Nugent et al. (1995) employed a simple approach by drawing straight lines at the local peaks of the spectral features and measuring the depth of the absorption minima from the straight line. However, the location of the straight line and the position of the line minimum are not easy to define in the presence of observational errors. It is for these reasons the ratios are derived only for a number of very well-observed local SNe. Another measure of feature strength is based on pseudo-EWs. Here, the continuum level is estimated by finding the maxima on either side of the feature and a straight line is drawn to connect the two maxima. This line is used as the continuum level. In the past, the maxima have been found either by eye (Nugent et al. 1995; Branch et al. 2006) or by a simple algorithm (Folatelli 2004; Garavini et al. 2007a). The EW is then calculated by finding the area and depth of the chosen region using the estimated continuum level. The problem with either of these methods is that the continuum is poorly estimated due to line blending and the P-Cygni profile of many SNe spectral features.

In this paper, the spectral features of Type Ia SNe will be analyzed through wavelet transformations. This technique avoids many of the challenges mentioned above associated with identifying line strengths. In particular, the wavelet technique obviates the need to define a continuum. Here wavelet transformations are applied to Type Ia SNe spectra with the purpose of quantifying spectral features for cosmological applications.

2. SPECTRAL FEATURES

2.1. Wavelet Transform Algorithm

Wavelet decomposition, like Fourier decomposition, expresses a given function in terms of the superposition of a set of simple basis functions. Unlike Fourier decomposition, individual wavelet functions are localized in the spatial domain on a scale that is variable. The transform is carried out in direct space so artifacts related to periodicity are avoided. The reconstruction is trivial and again, unlike the Fourier decomposition, there are a finite number of wavelet scales so that the original function can be restored without distortion. The evolution of the transform from one scale to the next is easy to follow and interpretation of the spectrum at each scale straightforward.

There are a large number of functions that can be used for the wavelet transform. It has been previously demonstrated that the *à trous* algorithm is a particularly useful tool for studying spectral features (Holtschneider et al. 1989; Shensa 1992; Starck et al. 1995, 1997) and is thus adopted for our purposes. Taken literally, the French term *à trous* is interpreted as "with holes," expressing the fact that convolution is interlaced. That is, the convolution mask retains the same number of points but increases in scale as the decomposition evolves, resulting in holes within the convolution mask. Assuming a scaling function $\phi(x)$ (which corresponds to a low pass filter—also called the convolution mask), the first filtering is performed on the original data $c_0(k)$ to generate $c_1(k)$. The signal difference $c_0(k) - c_1(k)$ is the wavelet scale $w_1(k)$ and contains the information between these two scales (in this case the point-to-point variation within the data). This operation is performed successively to obtain the wavelet scale $w_j(k)$ at each scale j until scale J is reached, where

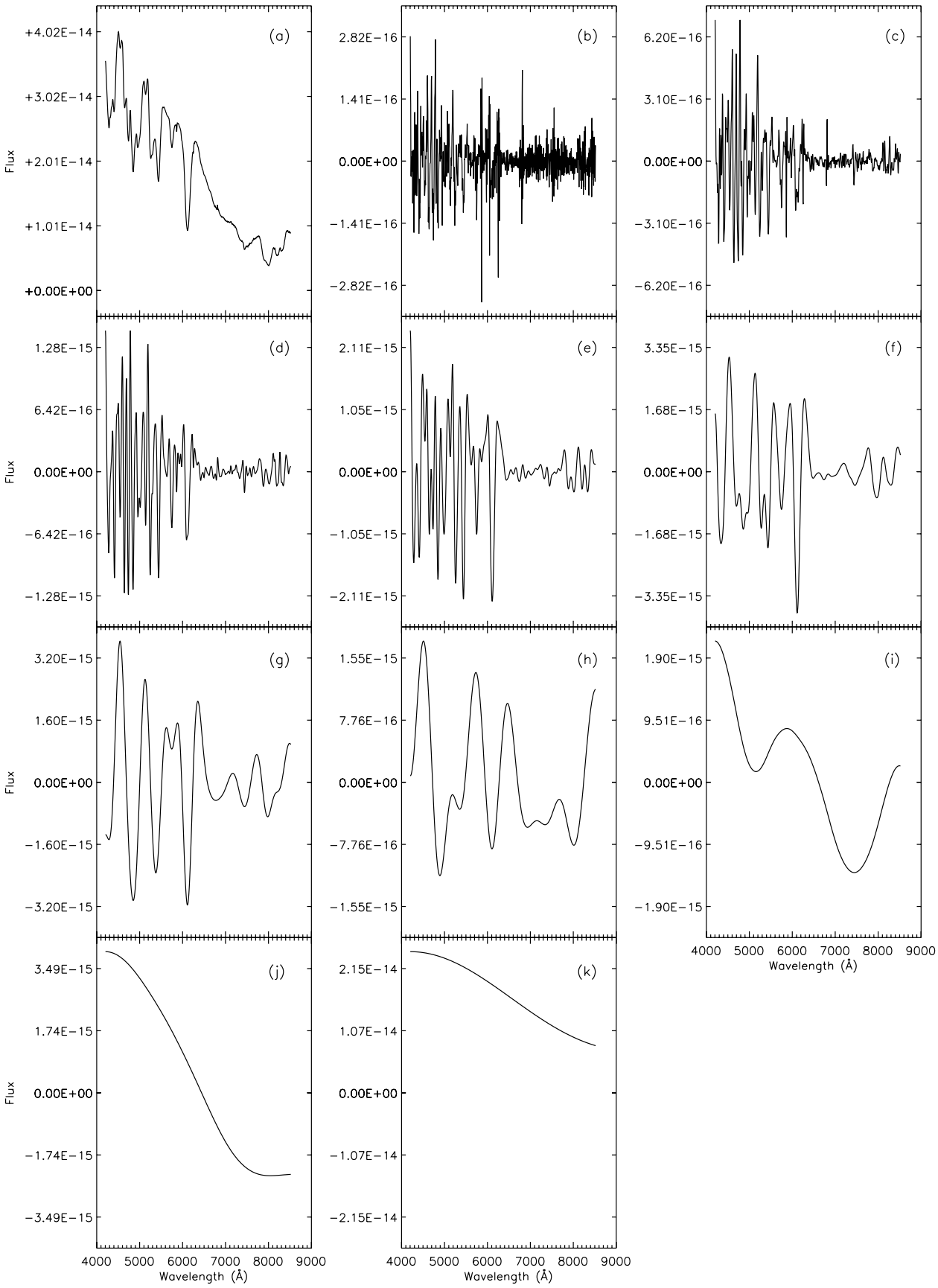

Figure 1. (a) Spectrum of SN 2001el, ((b)–(j)) the wavelet scales 1–9, and (k) the smoothed array c_p of the SN 2001el. A sum of scales (b)–(k) recovers the original spectrum (a). The mean fluxes of each of the wavelet scales (b)–(j) are identically zero.

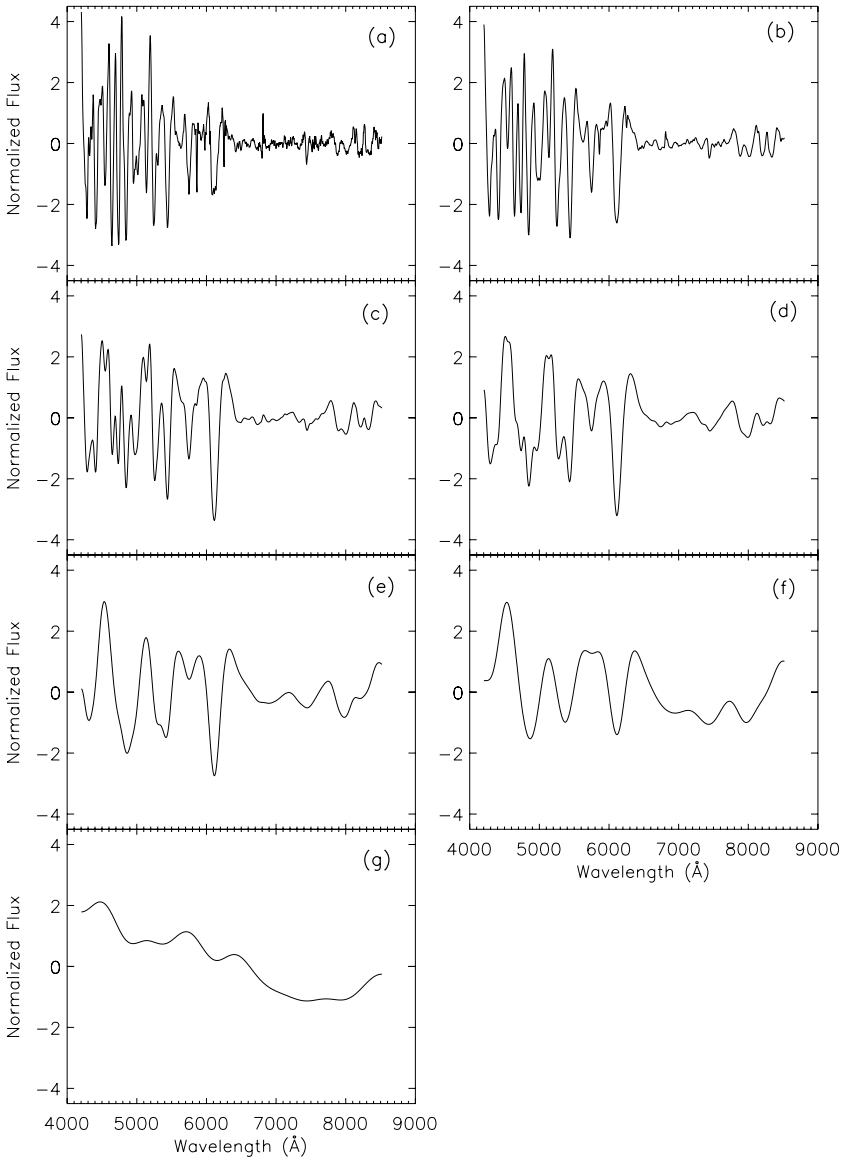

Figure 2. Wavelet sums for SN 2001el over (a) scales 1–3, (b) 2–4, (c) 3–5, (d) 4–6, (e) 5–7, (f) 6–8, and (g) 7–9. Running combinations of the different scales capture features of varying width.

2^J is equal to the number of data points. The original spectrum c_0 can be expressed as the sum of all the wavelet scales and the last smoothed array c_J:

$$c_0(k) = c_J(k) + \Sigma_{J=1}^{J-1} w_j(k).$$

To demonstrate the basic features of the *à trous* wavelet transformation, we show in Figure 1 the wavelet transformation of the well-observed supernova SN 2001el. These data were obtained through the spectropolarimetry program at the Very Large Telescope (VLT) of the European Southern Observatory (ESO; Wang et al. 2003) but are rebinned here to 5 Å. The signal-to-noise ratio (S/N) of the data is everywhere above 150—this unusually high S/N is a result of the spectropolarimetry observations. The original data are shown in Figure 1(a), and the consecutive wavelet scales for $j = 1$, 9 are shown in Figures 1(b)–(j). Figure 1(k) represents the smoothed array c_p.

We now consider the wavelet transformation in greater detail. The number of 5 Å bins in the original SN 2001el spectrum taken 1 day after *B*-band maximum is 864. In order to use the *à trous* algorithm the data must have 2^J data points—to meet this requirement the spectrum was padded at the red end with a decaying exponential so that the data have 2^{10} data points, giving $J = 10$ but allowing only nine wavelet scales. The convolution mask for the *à trous* wavelet used throughout this paper is a symmetric triangle function applied at five bins within the spectrum, with weights 0.3875, 0.25, and 0.0625. Initially, all five points of the convolution function are adjacent to one another. This function is then convolved with c_0, the function advanced by one bin and repeated until the end of the spectrum is reached. The 1024 bins comprising the convolved data are subtracted from c_0 to generate c_1. To generate c_2, the convolution function is magnified by a factor of 2 (leaving a gap of one bin between adjacent points in the original filter) and the process repeated until the original convolution factor has been expanded by a factor of 8.

Various properties of the wavelet transform are observed in Figure 1. It is seen that at small scales the wavelet is dominated by observational noise. The SN signal starts to become significant only for $j \geqslant 3$, and the broad spectral

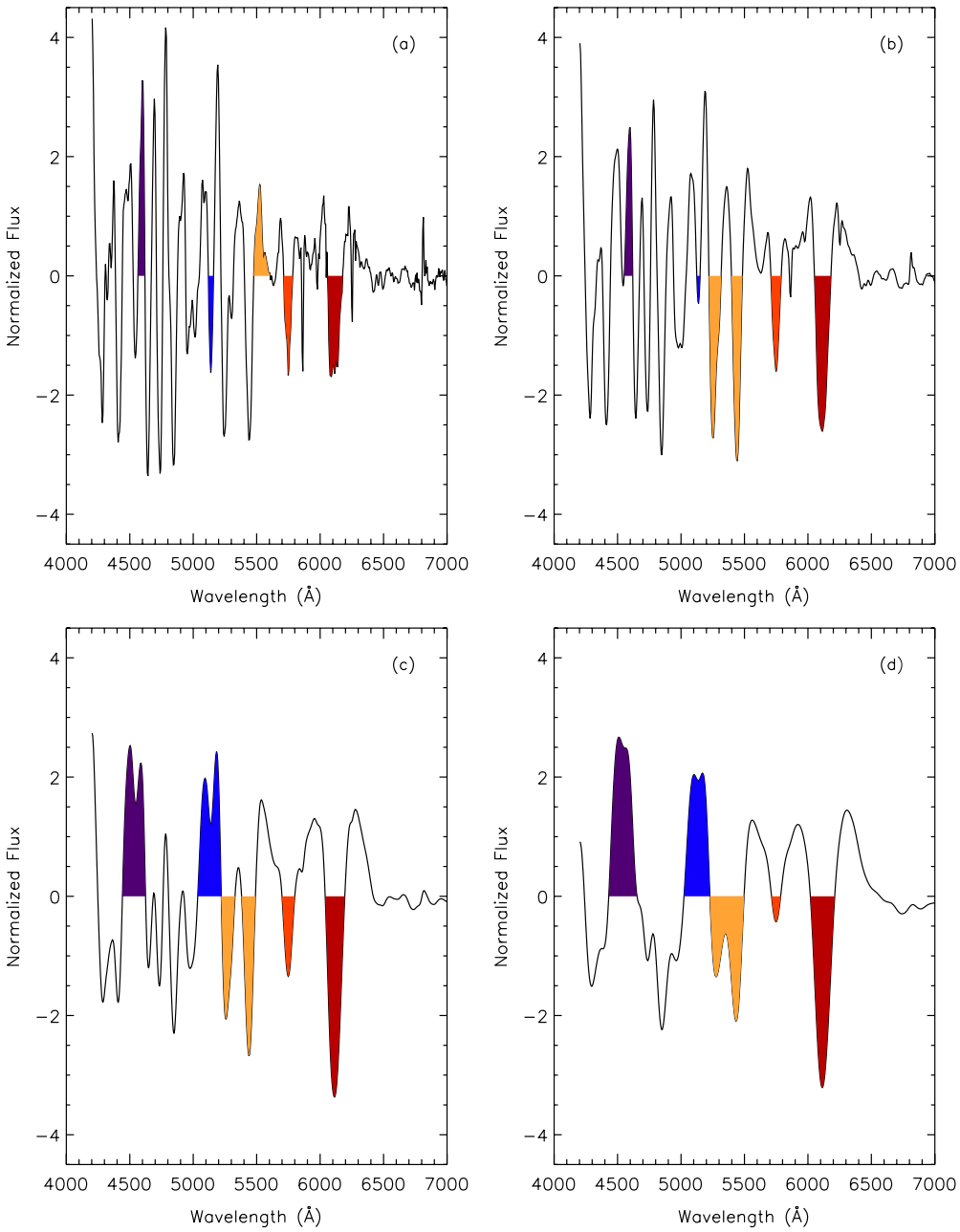

Figure 3. Spectral features for Type Ia SNe. (a) $l = 1, 2, 3$; (b) $l = 2, 3, 4$, (c) $l = 3, 4, 5$, and (d) $l = 4, 5, 6$. The spectral features are well resolved in (c) and (d). (A color version of this figure is available in the online journal.)

wiggles associated with the SN dominate the wavelet scales of $j = 5$, 6, and 7. The SN spectral features are typically a few hundred Å wide and are effectively isolated in the decomposed spectra. We note that each of the individual wavelet scales has zero mean.

The spectral features of a SN are better described by a blend of several wavelet scales. For this reason, we can calculate the sum of more than one scales to reflect the existence of features of various width:

$$W_{\{l\}} = \Sigma_{j\in\{l\}} w_j,$$

where $\{l\}$ is a subset of wavelet scales. Examples of these sums are shown in Figure 2 for SN 2001el.

2.2. *Normalization of Spectral Features*

Retaining the units of the original flux spectrum, the wavelet scales need to be normalized to construct quantities that measure spectral features strength independent of the absolute flux level. While there undoubtedly is more than one way to normalize the scales, the simplest would be to normalize all the wavelet scales by dividing them by the smoothed array c_p. This approach is simple and will certainly work fine for data without host galaxy contamination. For data with host galaxy contamination, or those with poor background subtraction, this approach introduces systematic errors to the normalized scales.

In our approach, the normalized wavelet scale is defined using the standard deviations of the spectral features from any given

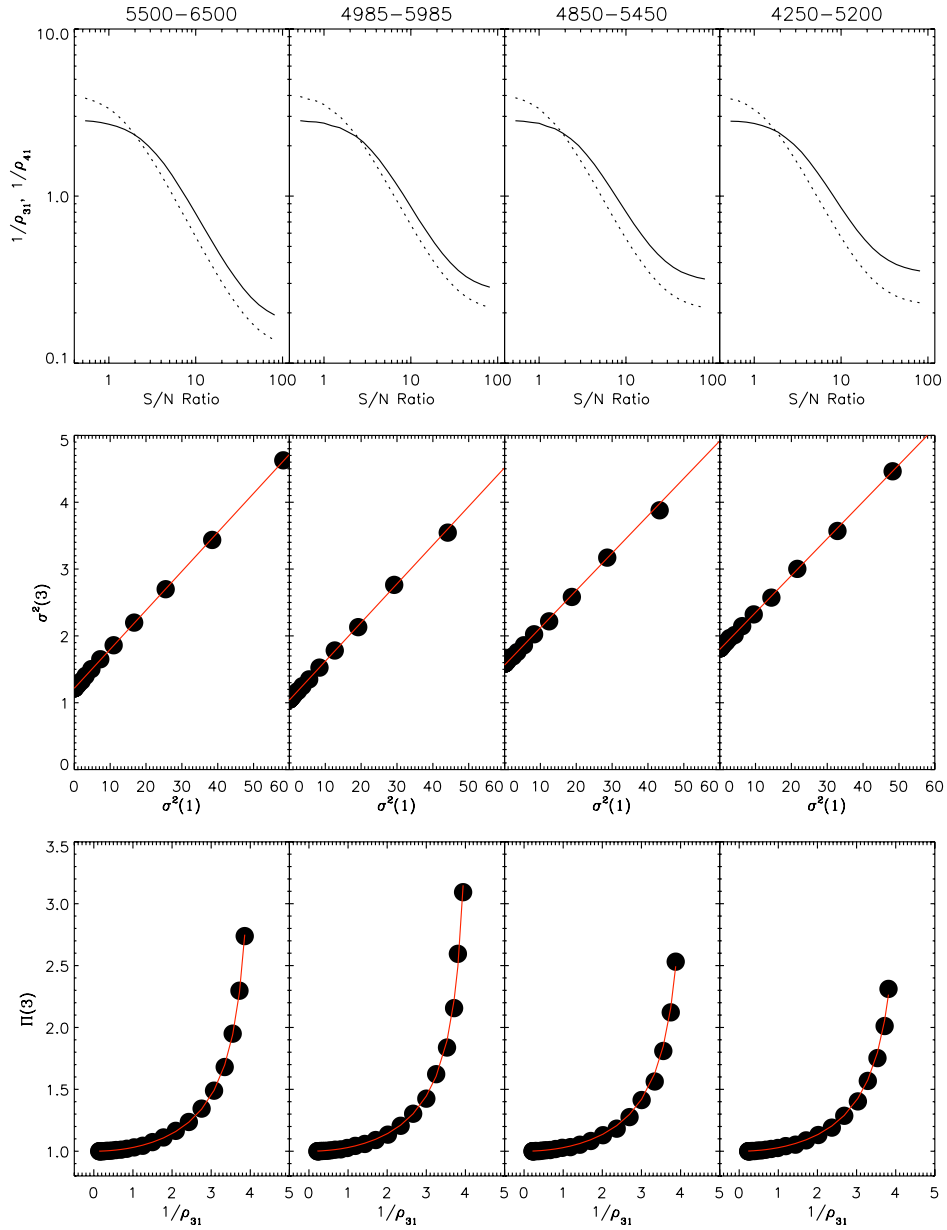

Figure 4. Top: relation between the SQI and input S/N ratios. The solid lines show SQI of fourth wavelet scale and the dashed line the third. Middle: relation between the variance of the third and first wavelet scales. The effect of a large $\sigma(1)$ propagates linearly to larger wavelet scales. Bottom: correlation of the bias correction factor and SQI for the third wavelet scale. The S/N was varied in all cases via the addition of noise in the Monte Carlo simulations.

(A color version of this figure is available in the online journal.)

Table 1
Zeroes (λ_a, λ_b) in the Normalized Flux for SN 2001el for the Five Features Described in the Text

Feature	λ_a	λ_b	$\lambda_{a'}$	$\lambda_{b'}$
6150	6038.75	6196.25		
5750	5698.75	5801.25		
5485	5378.75	5491.25	5218.75	5331.25
5150	5034.81	5222.31		
4570	4439.81	4624.81		

wavelet scale:

$$\hat{W}_{\{l\}}(\lambda) = W_{\{l\}}(\lambda) \Big/ \sqrt{\Sigma_{\lambda_1}^{\lambda_2} W_{\{l\}}^2(\lambda)/N_{12}} \quad (1)$$

$$= W_{\{l\}}(\lambda)/\sigma_{\{l\}}, \quad (2)$$

where N_{12} is the number of bins between λ_1 and λ_2 (explicitly defined below). The mean and standard deviation of $\hat{W}_{\{l\}}$ are zero and 1, respectively. This is effectively a self-normalization that exploits only the intrinsic properties of the wavelet scales involved. Host galaxy contamination (which does strongly affect c_p) would not have a significant effect in this context.

The spectral index X_j of any feature at a given scale j is defined by averaging the normalized wavelet scale $\hat{W}_j$:

$$X_{\{l\}} = \Sigma_{\lambda_a}^{\lambda_b} \hat{W}_{\{l\}}(\lambda)/N,$$

with N being the bin size in the wavelength region λ_a and λ_b, defined as the wavelengths corresponding to the leading and trailing zeros in the normalized flux of a feature, respectively (see Table 1 for SN 2001el).

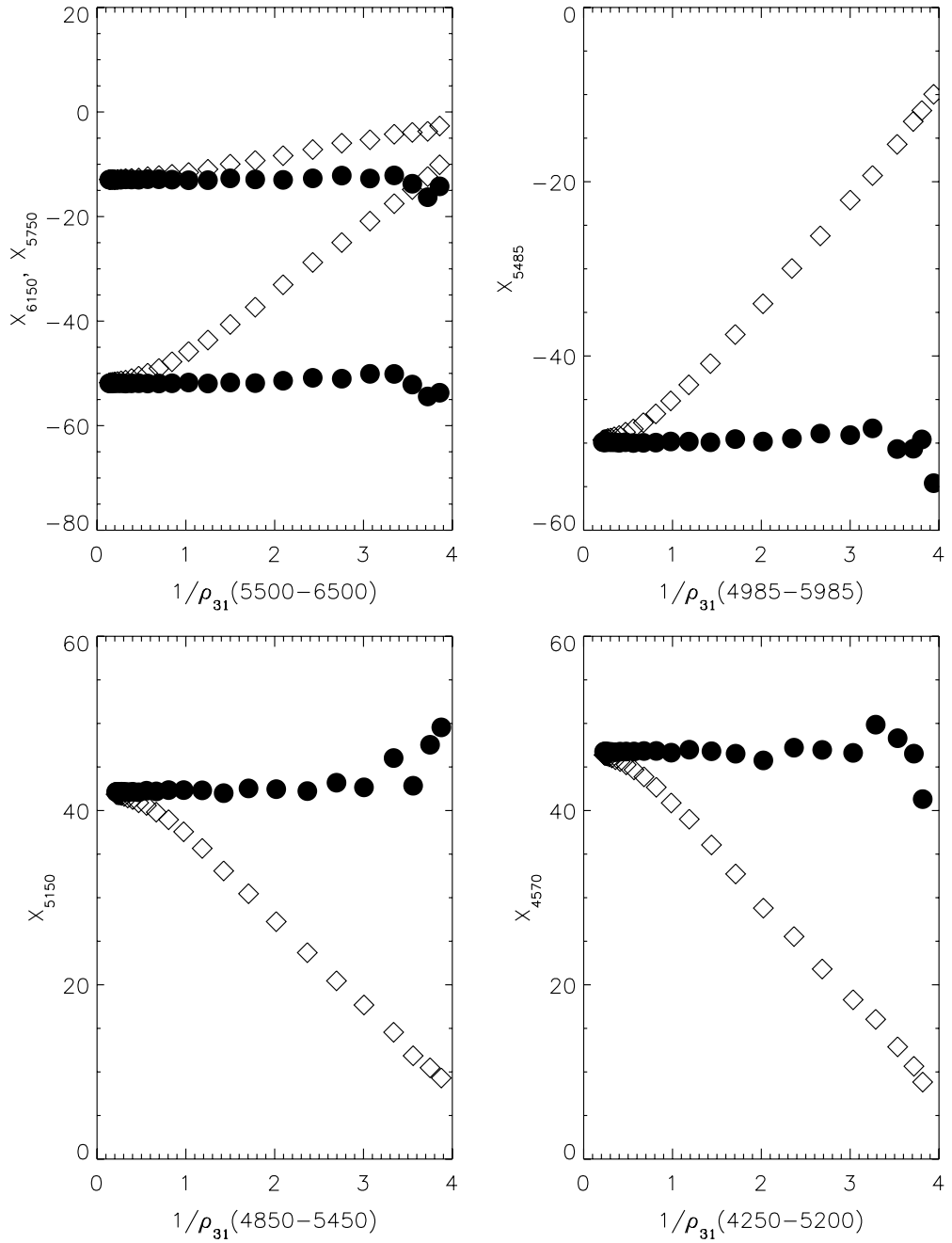

Figure 5. Spectral indices corrected (circles) for ρ dependence for important SN Type 1a spectral features. The X indices are derived from the sum of wavelets 3, 4, 5 of SN 2001el 1 day past optical maximum.

Table 2
The Coefficients for the Dependence of X on Data Errors

SN	Day	$\gamma_{31}(A)$	$\gamma_{31}(B)$	$\gamma_{31}(C)$	$\gamma_{31}(D)$	Mean	$\gamma_{41}(A)$	$\gamma_{41}(B)$	$\gamma_{41}(C)$	$\gamma_{41}(D)$	Mean
01V	−8	0.1132	0.1116	0.1183	0.1144	0.1144	0.0263	0.0240	0.0273	0.0259	0.0258
01el	−4	0.1220	0.1236	0.1229	0.1224	0.1227	0.0567	0.0587	0.0566	0.0573	0.0573
01el	+1	0.1220	0.1236	0.1229	0.1224	0.1227	0.0581	0.0583	0.0552	0.0551	0.0567
01el	+9	0.1251	0.1273	0.1250	0.1240	0.1254	0.0585	0.0607	0.0599	0.0577	0.0592

X_j defines a normalized number which measures the strength of the spectral features in the normalized wavelet scale $\hat{W}_j$ between λ_a and λ_b. Alternatively, one can also calculate the power P_j between λ_a and λ_b for wavelet scale j:

$$P_{\{l\}} = \Sigma_{\lambda_a}^{\lambda_b} \hat{W}_{\{l\}}^2(\lambda)/N_{ab}.$$

$P_{\{l\}}$ and $X_{\{l\}}$ contain the same information. In this study, we will focus on $X_{\{l\}}$.

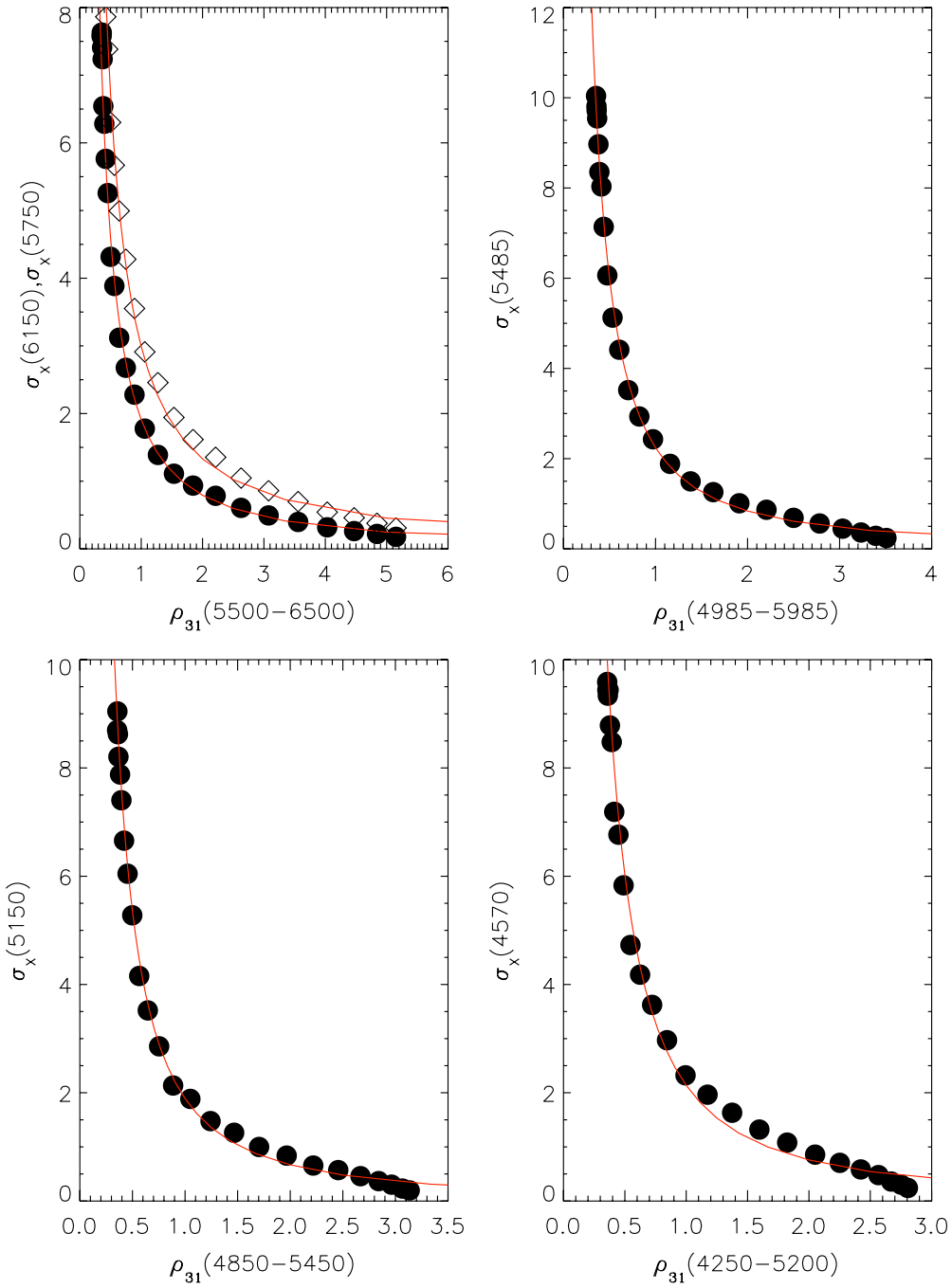

Figure 6. Errors of the X indices as functions of ρ for SN 2001el at optical maximum.
(A color version of this figure is available in the online journal.)

Table 3
The Coefficients for the Errors of X

SN	Date	$\eta(6150)$	$\psi(6150)$	$\eta(5800)$	$\psi(5800)$	$\eta(5485)$	$\psi(5485)$	$\eta(5150)$	$\psi(5150)$	$\eta(4250)$	$\psi(4250)$
2001V	−8	−0.02486	0.0469	−0.0156	0.0293	−0.0203	0.0601	−0.0373	0.0545	−0.0179	0.0453
2001el	−4	−0.00625	0. 0367	−0.00628	0.05429	−0.02449	0.05892	−0.01626	0.06382	−0.01165	0.05248
2001el	+1	0.133	1.248	0.212	1.188	0.160	1.412	0.176	1.533	0.157	1.531
2001el	+9	0.159	1.276	0.194	1.282	0.234	1.279	0.203	1.442	0.177	1.672
2001el	+1	0.145	1.194	0.265	1.322	0.175	1.295	0.181	1.500	0.216	1.408

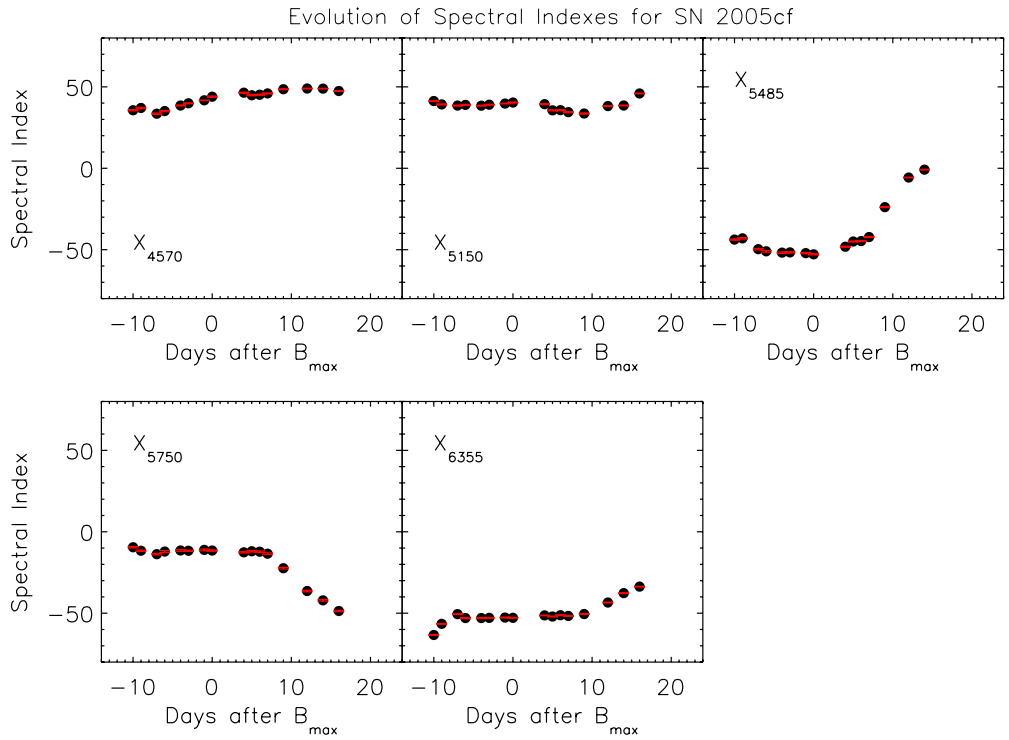

Figure 7. Temporal evolution of the *X* indices of SN 2005cf. In order these are (a) the emission feature at 4570 Å associated in part with the P Cygni profile of Mg II at 4471 Å, (b) the emission feature at 5150 associated in part with the P Cygni profile of Si II at 5041 Å, (c) the absorption "w" around 5485 Å associated around maximum with the S II 5433/5459 Å feature, (d) an absorption feature at 5750 Å associated around maximum with the Si II 5972 Å line, and (e) a strong absorption feature at 6150 Å associated around maximum with the Si II 6355 Å.

(A color version of this figure is available in the online journal.)

One obvious advantage to using wavelet scales to estimate spectral feature strengths is that they do not depend on the definition of the spectral continua. Furthermore, since they can be estimated locally around a spectral feature, spectral indices are useful in minimizing uncertainties due to errors in spectral flux calibration. Similarly, the spectral indices as defined here are less sensitive to errors of background subtraction—usually one of the dominant sources of uncertainty, especially in the studies of high redshift SNe. The wavelet technique is particularly suited for studying spectra dominated by scattering from expanding atmospheres with P-Cygni spectral features: the net flux of the P-Cygni feature is usually close to zero. Wavelet decomposition is consistent with this as the mean flux is zero for the various wavelet scales. Wavelet transforms thus make it easy to separate emission and absorption components of a spectrum in a mathematically robust way.

2.3. Normalization of SN Ia Spectral Features

In this study, the SN spectra are first decomposed into various scales as described in the previous section. In addition, to reflect the fact the spectral features are a blend of different scales, sums of the wavelet scales are used. All decomposed spectra are normalized according to Equation (2). To derive quantities that are less sensitive to flux calibration errors, we restrict the wavelength region used to calculate the normalization factor yet require it be large enough that spectral strengths are largely unaffected by the location of the boundary. In this study, the spectra are divided into four regions: (A) 5500–6500 Å, (B) 4985–5985 Å, (C) 4850–5450 Å, and (D) 4250–5200 Å; the variance in each of these sections of spectra is calculated and used as the normalization factor. These regions were chosen to incorporate the features listed below and are large enough to characterize the variance around each feature. Interesting features include the silicon II lines at 5972 and 6355 Å in region (A), the sulfur II lines at 5433 Å and 5459 Å in region (B), and two strong, clean emission features at 5150 Å and 4570 Å, in regions (C) and (D), respectively. The two emission features arise, in part, from P Cygni profiles of Si II at 5041 Å and Mg II at 4471 Å and are chosen as clean examples of emission features. These five (the 5433 Å and 5459 Å features are treated as a single feature) spectral features are shown in Figure 3 for various wavelet sums. We adopt the sums of wavelet scales 3, 4, and 5 for subsequent analyses.

3. BIASES AND ERRORS

In practice, the observed data contain noise and estimates of X_j can be biased. The noise affects X_j in two ways: first, when the noise is large, its effect can propagate to all the wavelet scales and become a significant component at the wavelet scale of interest. Second, it changes the normalization factor when calculating $\hat{W}_j$—data with larger noise can be systematically biased to give a larger normalization factor because the additional power from shot noise. This bias is usually not a problem for high S/N data, but can be significant for data with a low S/N. The correction factor $\Pi(j)$ for scale j is defined as

$$\sigma_0(j) = \sigma(j)\Pi_{1j}, \tag{3}$$

where $\sigma_0(j)$ is the variance at the jth scale in the ideal case of no photon shot noise.

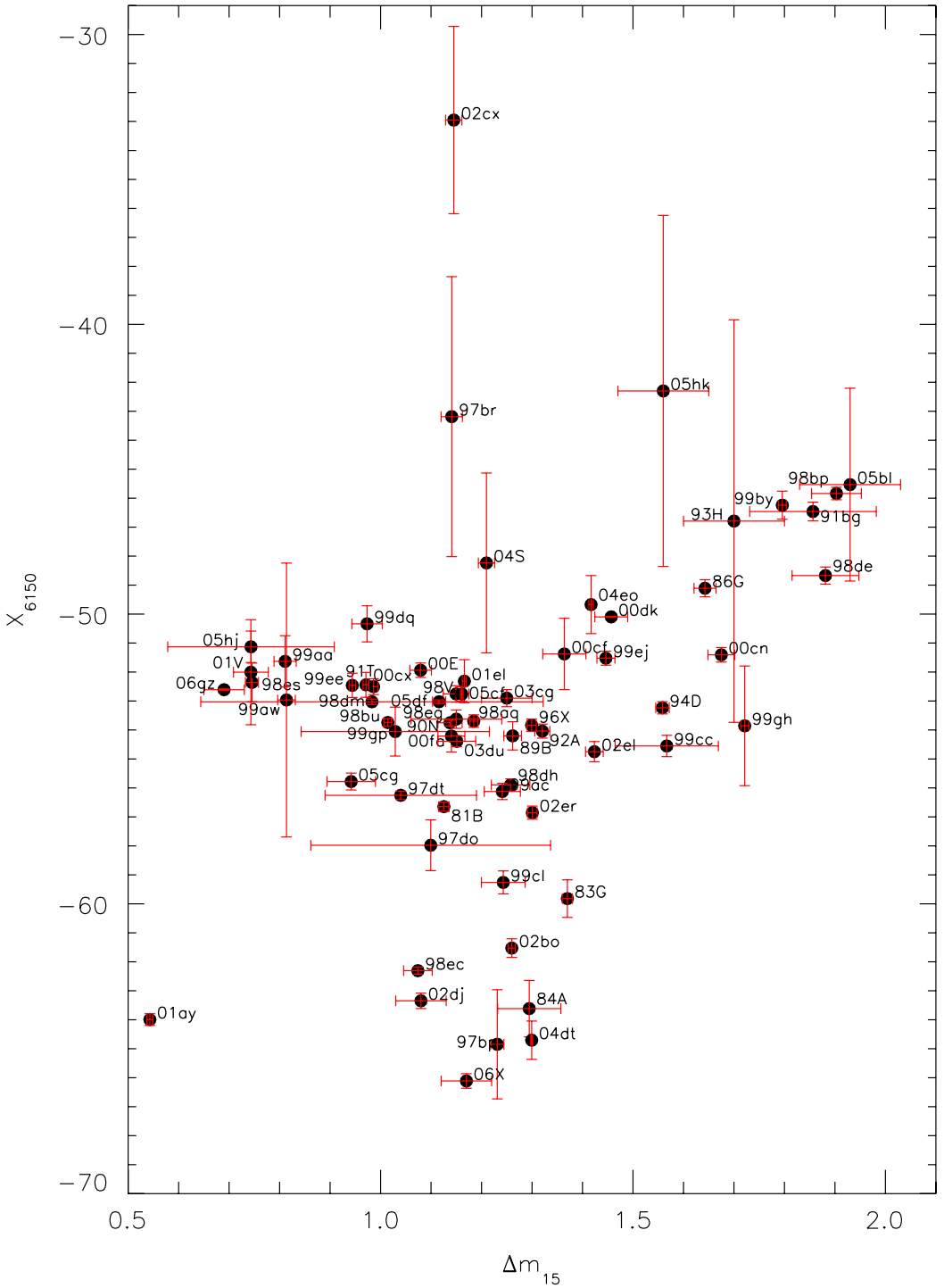

Figure 8. Correlation of the strength of X_{6150} (associated with the Si II 6355 Å feature) and Δm_{15}.
(A color version of this figure is available in the online journal.)

Typically, published spectroscopic data do not have associated noise spectra. One instead has to rely on the flux spectrum to estimate the noise levels. A major advantage of wavelet transformation is that it allows estimates of the noise characteristics based on the spectral data itself. If we assume that all the continuum or spectral features are much broader than the data sampling step, the spectral fluctuations of the wavelet scale with $j = 1$ should then represent mostly shot noise. This is generally reasonable as can be seen in Figure 1(b) for the spectrum of Type Ia SN 2001el.

Recognizing that smaller wavelet scales contain more information of the noise property than larger wavelet scales, we can define the spectral quality index (SQI) of the normalized wavelet scale $\{l\}$ as the variance ratio of normalized scale $\{l\}$ and the lowest normalized scale $\{1\}$:

$$\rho_{\{l\}\{1\}} = \Sigma_{\lambda_b}^{\lambda_a} \hat{W}_{\{l\}}^2 / \Sigma_{\lambda 1}^{\lambda 2} \hat{W}_{\{1\}}^2, \quad (4)$$

where the braces $\{\}$ reflect that the various quantities are actually sums of various wavelet scales. Specifically, $\hat{W}_{\{1\}}$ is

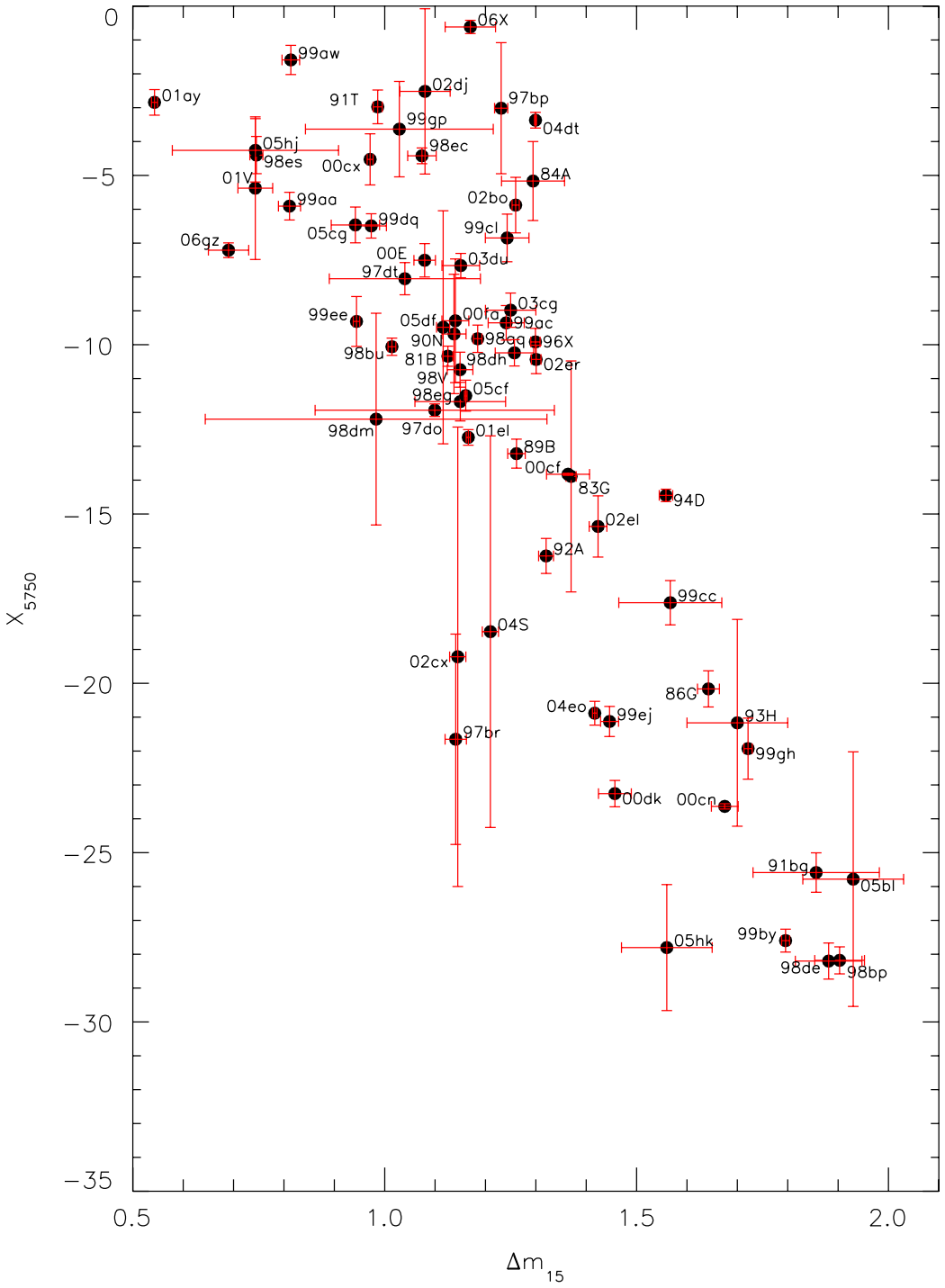

Figure 9. Correlation of the strength of X_{5750} (at maximum associated with Si II 5972) and Δm_{15}.
(A color version of this figure is available in the online journal.)

the normalized sum of three wavelet scales, where $\{l\} = 1, 2, 3$ in this instance. The SQI measures the relative importance of noise levels in estimating the spectral feature index. It can be calculated directly from the decomposed spectra without an error spectrum. Note that SQI is a quantity that can be localized to certain wavelength intervals.

For a given spectrum $\{c_i\}$, the dependence of the wavelet spectral indices $X_{\{l\}}$ and the correction factor Π on SQI can be estimated through Monte Carlo simulations.

3.1. Dependence of Spectral Features on Observational Noise

Monte Carlo simulations are required to quantify the dependence of the X indices on observational noise. The characteristic parameter of the noise is the SQI defined in Equation (4)—the ratio of spectral variance of combined wavelet scales $l = 3, 4, 5$ to that of the combined scales $l = 1, 2, 3$. To perform such simulations one needs a series of noise-free spectra of SN spectra. The spectropolarimetry program at the ESO VLT has acquired

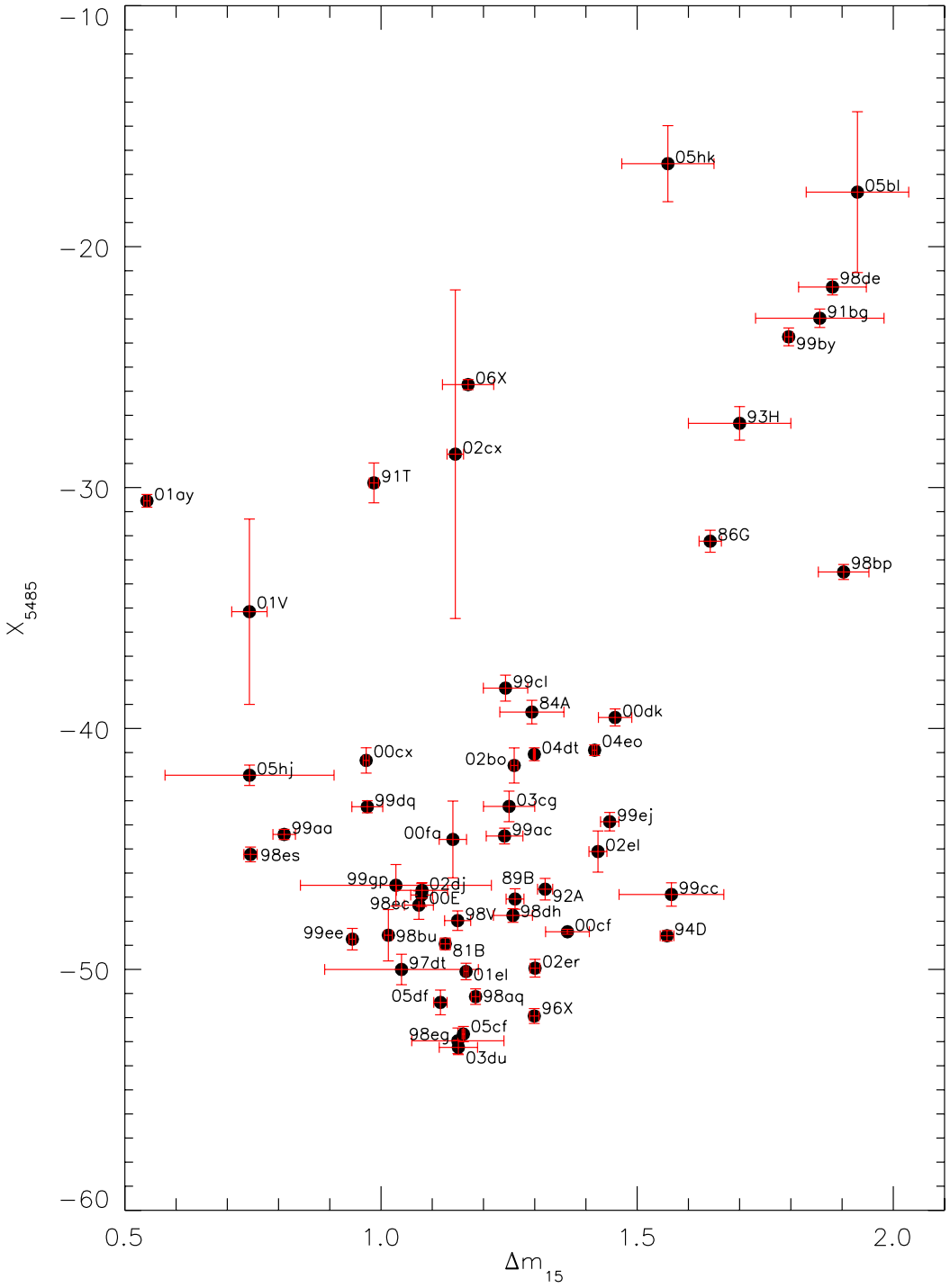

Figure 10. Correlation of the strength of X_{5485} (at maximum associated with S II 5433/5459 Å "w" feature) and Δm_{15}.
(A color version of this figure is available in the online journal.)

several high quality spectra of SN Ia with S/Ns around 150 (Wang et al. 2003). Spectra of SN 2001V and SN 2001el from the spectropolarimetry program will be used in this simulation to quantify the relations between X and SQI.

In the example shown in Figure 4, various levels of Poisson noises were added to the spectrum of SN 2001el at day +1. The noise is added to the spectra, which are then transformed to various wavelet scales and the various X indices are calculated. The top panel in Figure 4 shows the relation between ρ and the assumed S/N with the addition of Poisson noise. The SQI is calculated over the four distinct wavelength intervals defined in the previous section and as annotated in the top panel. It can be seen that ρ is correlates well with the S/N of the input data: ρ decreases as the S/N decreases. This confirms that the SQI can effectively capture effect the photon shot noise and can be used to quantify the noise level of the data.

The variances used to normalized the spectra at the various wavelet scales are clearly correlated. This is shown in the middle

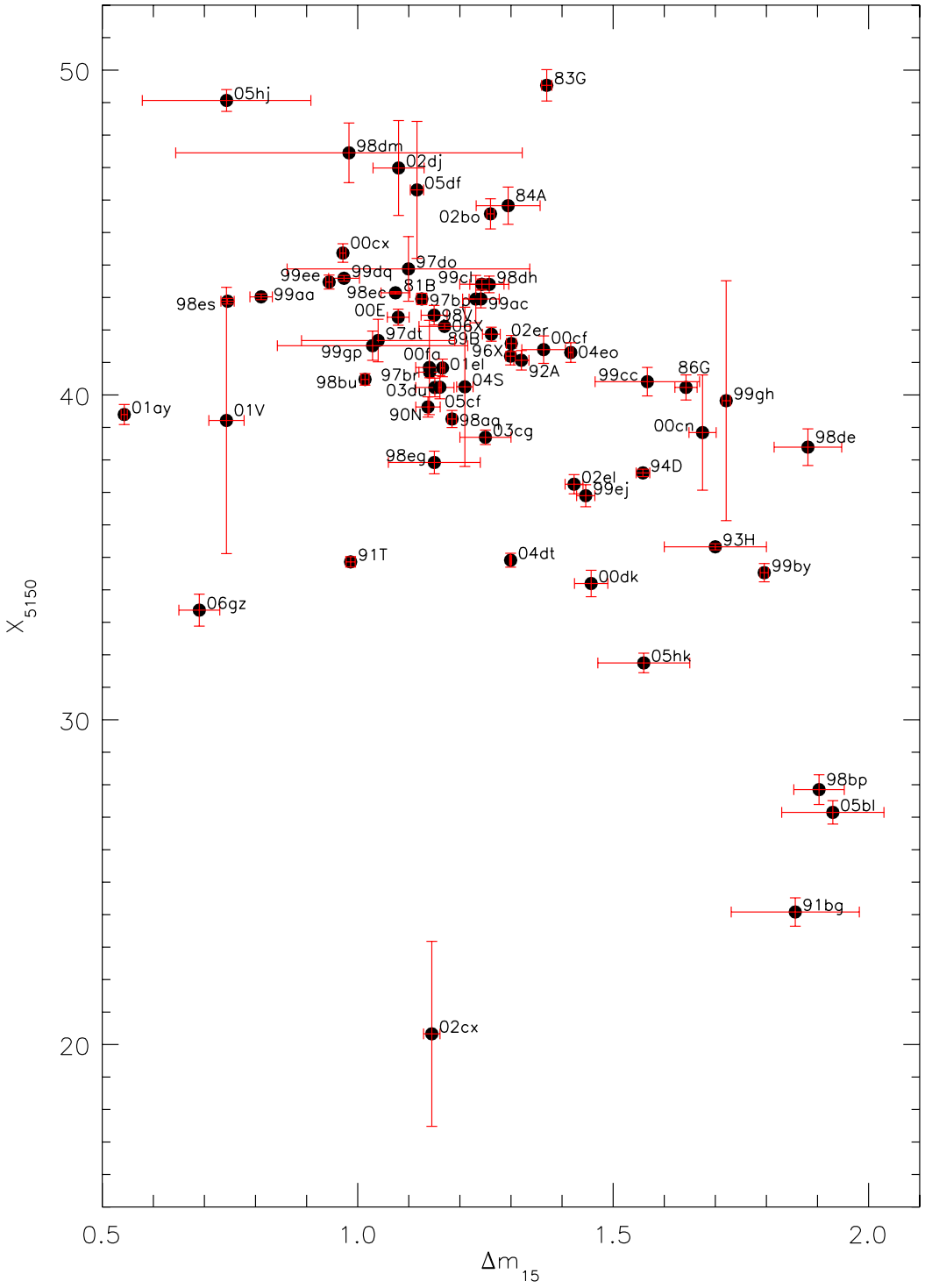

Figure 11. Correlation of the emission peak at 5150 Å and Δm_{15}.
(A color version of this figure is available in the online journal.)

panel of Figure 4, where the data exhibit nearly identical slopes over the different wavelength regions. A linear relationship between $\sigma^2(1)$ and $\sigma^2(3)$, and between $\sigma^2(1)$ and $\sigma^2(4)$ is assumed for the fits. The slopes γ_{1j} extracted from these fits are given in Table 2.

The bottom panel in Figure 4 clearly demonstrates how the correction factor Π increases dramatically as $1/\rho$ approaches 4 (corresponding to an S/N of below 1 per 5 Å bin). This implies that the spectral features are dominated by the noise, hence, it becomes impossible to extract the spectral indices reliably.

The correction factor for ρ can be fit well with a function

$$\Pi_{1j} = \sqrt{(1 - \gamma_{1j}\rho_{1j}^2)}, \quad (5)$$

with the relevant coefficients taken from Table 3 for the various lines.

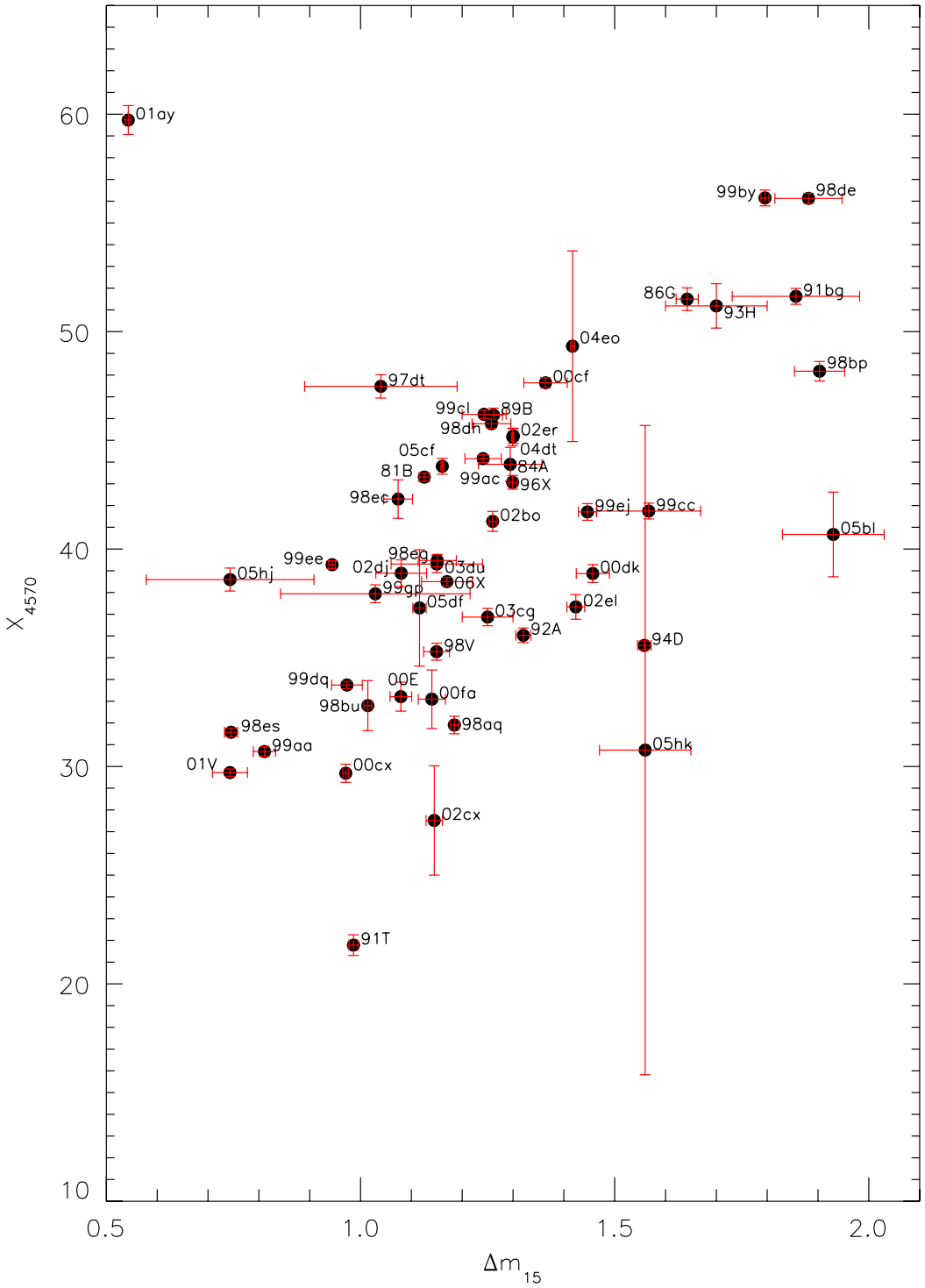

Figure 12. Correlation of the strength of the emission peak at 4570 Å and Δm_{15}.
(A color version of this figure is available in the online journal.)

3.2. Bias Corrections

The various X indices for the spectral features are derived from the Monte Carlo simulation of data with different SQIs. As shown in Figure 5, the X indices (shown as open squares) apparently suffer strong bias when the data are noisy. The various X indices after Π corrections are shown in Figure 5. The effect is generally small for high S/N data, but becomes important for data with low S/N. In any case the bias is effectively removed by applying the correction factor Π.

3.3. Error Estimates of the Spectral Indices

Assuming photon shot noise, the Monte Carlo simulations also give error estimates for the X indices. The errors as a function of ρ are shown in Figure 6. These errors are fitted

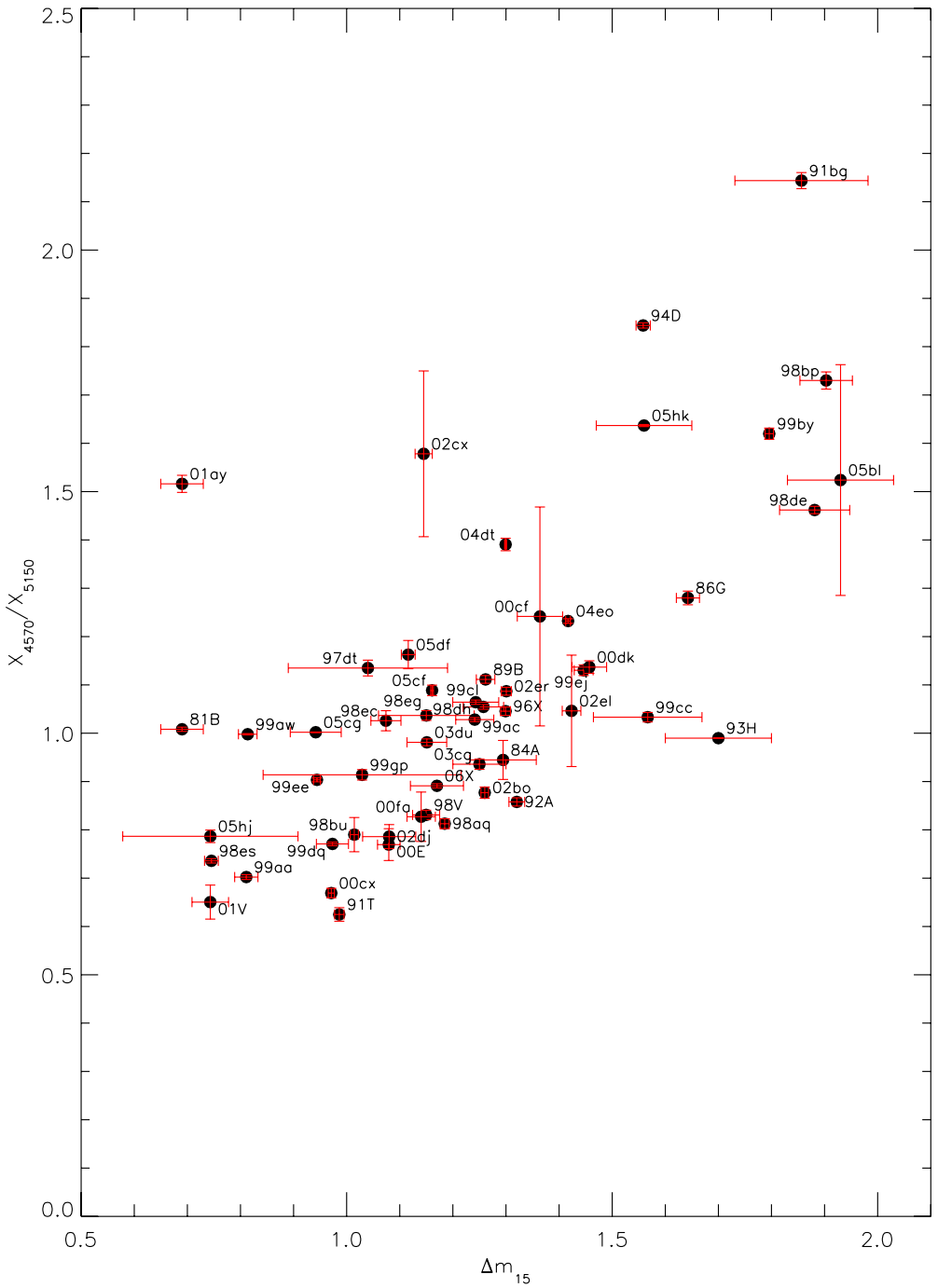

Figure 13. Correlation of the ratio of the strength of the emission peak at 4570 Å and 5150 Å and Δm_{15}.
(A color version of this figure is available in the online journal.)

with a function of the form:

$$\sigma_X = \eta \rho^{\psi}, \quad (6)$$

and the relevant coefficients η and ψ are shown in Table 3. Simulations were performed for all of the SN 2001V and SN 2001el spectra and it was found that in all cases the bias can be well corrected. Note that due to the lack of a completely noise-free SN Ia spectrum, at extremely high S/N (such as those that are higher than or comparable with the S/N of the SN 2001el spectra as used in the simulation) the Monte Carlo simulations do not give correct estimates of the errors. Such cases are unlikely to be relevant as in such situations the errors are likely to be dominated by calibration systematics rather than shot noise. As can be seen in Figure 6, the above expression gives an excellent description of the dependence when the errors are described by ρ.

The ρ dependence of the X indices and their errors have a weak dependence across the different varieties of SNe and their epochs.

3.3.1. Procedure for Bias and Error Estimation

The procedure for removing bias and estimating errors from noisy SNe spectra is premised on extracting correction factors from a SN with a large S/N. Here we enumerate a correction

Table 4
The Spectroscopic Sample of SNe Ia

SNe	Δm_{15}[a]	Branch Subtype[b]	X_{6150}	X_{5750}	X_{5485}	X_{5150}	X_{4570}	Spectra Source
1981B	1.125(0.010)	BL	−56.645(0.157)	−10.339(0.298)	−48.941(0.245)	42.956(0.175)	43.306(0.184)	1
1983G	1.37(0.01)[b]	...	−59.818(0.649)	−13.890(3.411)	... [c]	49.532(0.483)	... [c]	2
1984A	1.294(0.063)	BL	−63.615(0.974)	−5.166(1.167)	−39.319(0.489)	45.827(0.573)	43.895(0.781)	3
1986G	1.643(0.022)	CL	−49.109(0.295)	−20.165(0.534)	−32.227(0.456)	40.231(0.386)	51.494(0.521)	4
1989B	1.262(0.017)	CL	−54.202(0.486)	−13.218(0.428)	−47.078(0.424)	41.870(0.216)	46.161(0.318)	5, 6
1990N	1.138(0.024)	CN	−53.751(0.112)	−9.683(1.763)	... [c]	39.630(0.312)	... [c]	7, 8
1991T	0.986(0.009)	SS	−52.505(0.274)	−2.976(0.499)	−29.806(0.829)	34.860(0.159)	21.783(0.474)	9, 10, 11
1991bg	1.857(0.125)	CL	−46.461(0.324)	−25.588(0.582)	−22.972(0.382)	24.081(0.436)	51.622(0.367)	12, 13, 14
1992A	1.320(0.015)	BL	−54.040(0.242)	−16.239(0.517)	−46.671(0.447)	41.067(0.300)	36.031(0.336)	15
1993H	1.70(0.10)[d]	...	−46.790(6.947)	−21.166(3.053)	−27.335(0.697)	35.324(0.093)	51.183(1.020)	16
1994D	1.558(0.013)	CN	−53.234(0.212)	−14.450(0.182)	−48.604(0.216)	37.600(0.114)	35.566(0.207)	17, 18
1996X	1.299(0.009)	CN	−53.837(0.216)	−9.917(0.400)	−51.935(0.309)	41.193(0.271)	43.070(0.317)	19, 20
1997bp	1.231(0.013)	...	−64.847(1.884)	−3.015(1.935)	... [c]	42.951(0.729)	... [c]	21
1997br	1.141(0.021)	SS	−43.186(4.832)	−21.652(3.106)	... [c]	40.701(0.171)	... [c]	22
1997do	1.099(0.237)	BL	−57.978(0.878)	−11.934(0.186)	... [c]	43.880(0.995)	... [c]	23
1997dt	1.04(0.15)[e]	CN	−56.255(0.148)	−8.051(0.475)	−50.003(0.632)	41.675(0.655)	47.482(0.538)	23
1998V	1.150(0.025)	CN	−52.756(0.285)	−10.737(0.517)	−47.976(0.406)	42.455(0.300)	35.278(0.390)	23
1998aq	1.185(0.008)	CN	−53.695(0.218)	−9.824(0.404)	−51.130(0.322)	39.259(0.262)	31.908(0.403)	23, 24
1998bp	1.903(0.013)	CL	−45.839(0.215)	−28.182(0.399)	−33.504(0.312)	27.849(0.458)	48.179(0.449)	23
1998bu	1.014(0.008)	CN	−53.743(0.137)	−10.060(0.255)	−48.582(1.067)	40.477(0.177)	32.800(1.149)	23, 25, 26, 27
1998de	1.881(0.066)	CL	−48.672(0.294)	−28.202(0.533)	−21.675(0.329)	38.392(0.564)	56.127(0.232)	23
1998dh	1.258(0.038)	BL	−55.895(0.209)	−10.240(0.388)	−47.762(0.285)	43.403(0.257)	45.766(0.205)	23
1998dm	0.983(0.339)	...	−53.027(0.094)	−12.198(3.126)	... [c]	47.453(0.919)	... [c]	23
1998ec	1.074(0.028)	BL	−62.305(0.121)	−4.422(0.232)	−47.332(0.591)	43.144(0.037)	42.297(0.887)	23
1998eg	1.15(0.09)[f]	CN	−53.627(0.317)	−11.681(0.570)	−52.964(0.531)	37.920(0.349)	39.311(0.394)	23
1998es	0.745(0.013)	SS	−52.360(0.668)	−4.399(0.549)	−45.227(0.306)	42.884(0.086)	31.574(0.194)	23
1999aa	0.811(0.014)	SS	−51.631(0.885)	−5.908(0.408)	−44.397(0.210)	43.020(0.087)	30.685(0.214)	23, 28
1999ac	1.241(0.036)	SS	−56.123(0.280)	−9.354(0.509)	−44.465(0.327)	42.953(0.272)	44.159(0.183)	23, 29
1999aw	0.814(0.018)	SS	−52.965(4.726)	−1.590(0.431)	... [g]	... [g]	... [g]	30
1999by	1.796(0.008)	CL	−46.242(0.484)	−27.599(0.338)	−23.743(0.369)	34.528(0.282)	56.148(0.363)	23
1999cc	1.567(0.102)	BL	−54.551(0.368)	−17.619(0.654)	−46.891(0.486)	40.408(0.439)	41.747(0.363)	23
1999cl	1.243(0.043)	BL	−59.260(0.397)	−6.847(0.703)	−38.325(0.538)	43.409(0.161)	46.195(0.193)	23
1999dq	0.973(0.030)	SS	−50.336(0.623)	−6.492(0.359)	−43.249(0.249)	43.592(0.086)	33.746(0.162)	23
1999ee	0.944(0.006)	SS	−52.461(0.418)	−9.313(0.737)	−48.746(0.446)	43.475(0.215)	39.278(0.177)	31
1999ej	1.446(0.018)	BL	−51.523(0.241)	−21.127(0.443)	−43.869(0.384)	36.897(0.338)	41.707(0.383)	23
1999gh	1.721(0.008)	BL	−53.856(2.065)	−21.929(0.901)	... [c]	39.822(3.692)	... [c]	23
1999gp	1.029(0.186)	SS	−54.055(0.844)	−3.634(1.409)	−46.510(0.863)	41.516(0.449)	37.941(0.408)	23
2000E	1.079(0.021)	SS	−51.938(0.250)	−7.507(0.493)	−46.913(0.479)	42.393(0.248)	33.210(0.667)	32
2000cf	1.364(0.043)	...	−51.376(1.230)	−13.827(0.031)	−48.438(0.101)	41.395(0.424)	47.646(0.232)	23
2000cn	1.675(0.027)	CL	−51.405(0.250)	−23.634(0.078)	... [c]	38.841(1.773)	... [c]	23
2000cx	0.971(0.006)	SS	−52.441(0.429)	−4.527(0.755)	−41.327(0.525)	44.369(0.285)	29.687(0.418)	23, 33
2000dk	1.457(0.033)	CL	−50.096(0.017)	−23.257(0.389)	−39.544(0.354)	34.195(0.406)	38.875(0.413)	23
2000fa	1.140(0.027)	CN	−54.210(0.551)	−9.293(1.827)	−44.606(1.594)	40.845(1.452)	33.094(1.348)	23
2001V	0.743(0.034)	SS	−52.006(1.813)	−5.376(2.106)	−35.152(3.846)	39.213(4.099)	29.718(0.170)	23
2001ay	0.543(0.006)	BL	−63.993(0.203)	−2.843(0.378)	−30.552(0.265)	39.397(0.309)	59.731(0.666)	34
2001el	1.166(0.004)	CN	−52.317(0.744)	−12.737(0.230)	−50.087(0.342)	40.832(0.272)	... [h]	35
2002bo	1.260(0.007)	BL	−61.527(0.322)	−5.877(0.821)	−41.535(0.730)	45.575(0.464)	41.272(0.458)	36
2002cx	1.145(0.016)	SS	−32.952(3.231)	−19.216(6.785)	−28.614(6.820)	20.330(2.847)	27.516(2.514)	37
2002dj	1.08(0.05)[i]	BL	−63.346(0.267)	−2.519(2.441)	−46.720(0.321)	46.987(1.460)	38.889(0.614)	38
2002el	1.423(0.018)	...	−54.749(0.349)	−15.368(0.904)	−45.108(0.855)	37.251(0.296)	37.339(0.567)	39
2002er	1.301(0.009)	BL	−56.853(0.227)	−10.436(0.420)	−49.949(0.369)	41.584(0.248)	45.197(0.332)	40
2003cg	1.25(0.05)	CN	−52.901(0.295)	−8.980(0.506)	−43.235(0.634)	38.695(0.223)	36.871(0.400)	41
2003du	1.151(0.037)	CN	−54.388(0.192)	−7.664(0.360)	−53.238(0.300)	40.229(0.287)	39.471(0.283)	42, 43
2004S	1.210(0.016)	CN	−48.235(3.103)	−18.474(5.782)	... [c]	40.250(2.452)	... [c]	45
2004dt	1.299(0.002)	BL	−64.706(0.662)	−3.370(0.231)	−41.069(0.266)	34.912(0.214)	45.159(0.400)	46
2004eo	1.417(0.004)	CL	−49.673(1.001)	−20.883(0.351)	−40.903(0.220)	41.306(0.303)	49.330(4.384)	47
2005bl	1.93(0.10)	CL	−45.532(3.327)	−25.784(3.759)	−17.737(3.337)	27.149(0.361)	40.669(1.949)	48
2005cf	1.161(0.006)	CN	−52.758(0.249)	−11.505(0.457)	−52.686(0.316)	40.237(0.356)	43.805(0.364)	49
2005cg	0.942(0.048)[j]	SS	−55.780(0.292)	−6.463(0.528)	... [k]	... [k]	... [k]	50
2005df	1.116(0.013)	...	−53.024(0.064)	−9.486(3.441)	−51.371(0.514)	46.312(2.108)	37.292(2.676)	51
2005hj	0.743(0.165)[l]	SS	−51.129(0.542)	−4.260(0.935)	−41.942(0.423)	49.066(0.336)	38.596(0.529)	52
2005hk	1.56(0.09)[f]	SS	−42.299(6.056)	−27.804(1.861)	−16.555(1.580)	31.749(0.302)	30.752(14.932)	53
2006gz	0.69(0.04)[m]	SS	−52.610(0.032)	−7.209(0.217)	... [c]	33.375(0.492)	... [c]	54
2006X	1.17(0.04)[n]	BL	−66.111(0.252)	−0.616(0.195)	−25.726(0.209)	42.110(0.088)	38.500(0.186)	55

Table 4
(Continued)

Notes.
[a] Δm_{15} values were calculated by the super-stretch method from Wang et al. (2006b) unless otherwise noted.
[b] Designations from Branch et al. (2009).
[c] The 5485 Å and 4570 Å features show much more variance in their evolution, therefore the epoch range over which these features were fit was smaller. These SNe are missing X_{5485} and X_{4570} values because they did not have enough spectra within the smaller epoch range.
[d] Δm_{15} from Hachinger et al. (2006).
[e] Δm_{15} from Jha et al. (1999).
[f] Δm_{15} from Phillips et al. (2007).
[g] Due to noise or miscalibration of the spectra at +3 days, there is not enough data to fit X_{5485}, X_{5150}, and X_{4570}.
[h] The spectra for SN 2001el did not cover the wavelength region for this feature.
[i] Δm_{15} from Pignata et al. (2008).
[j] Δm_{15} converted from stretch value, s, from Quimby et al. (2006) using the equation from Perlmutter et al. (1997).
[k] Not enough of the spectra for SN 2005bl covered the wavelength regions for X_{5485}, X_{5150}, and X_{4570} for a good fit to be made.
[l] Δm_{15} converted from stretch value, s, from Quimby et al. (2007) using the equation from Perlmutter et al. (1997).
[m] Δm_{15} from Hicken et al. (2007).
[n] Δm_{15} from Wang et al. (2008).
References. (1) Branch et al. 1983; (2) Harris et al. 1983; (3) Barbon et al. 1989; (4) Phillips et al. 1987; (5) Barbon et al. 1990; (6) Wells et al. 1994; (7) Mazzali et al. 1993; (8) Leibundgut et al. 1991; (9) Filippenko et al. 1992a; (10) Phillips et al. 1992; (11) Ruiz-Lapuente et al. 1992; (12) Leibundgut et al. 1993; (13) Filippenko et al. 1992b; (14) Turatto et al. 1996; (15) Kirshner et al. 1993; (16) Wang unpublished; (17) Meikle et al. 1996; (18) Patat et al. 1996; (19) Wang et al. 1997; (20) Salvo et al. 2001; (21) Anupama 1997; (22) Li et al. 1999; (23) Matheson et al. 2008; (24) Branch et al. 2003; (25) Jha et al. 1999; (26) Meikle & Hernandez 2000; (27) Hernandez et al. 2000; (28) Garavini et al. 2004; (29) Garavini et al. 2005; (30) Strolger et al. 2002; (31) Hamuy et al. 2002; (32) Valentini et al. 2003; (33) Li et al. 2001; (34) Branch et al. 2006; (35) Wang et al. 2003; (36) Benetti et al. 2004; (37) Li et al. 2003; (38) Pignata et al. 2008; (39) Wang unpublished; (40) Kotak et al. 2005; (41) Elias-Rosa et al. 2006; (42) Anupama et al. 2005; (43) Stanishev et al. 2007; (44) Howell et al. 2006; (45) Krisciunas et al. 2007; (46) Altavilla et al. 2007; (47) Mazzali et al. 2008; (48) Taubenberger et al. 2008; (49) Garavini et al. 2007b; (50) Quimby et al. 2006; (51) Quain in progress; (52) Quimby et al. 2007; (53) Phillips et al. 2007; (54) Hicken et al. 2007; (55) Wang et al. 2008.

recipe using wavelet scales $l = 3, 4, 5$ with SN 2001el as our reference spectrum.

1. Compute the ratio of the sum of the squares of wavelet scales 3, 4, 5 and 1, 2, 3 (ρ_{31} in Equation (4)) for SN 2001el
$$\rho_{31} = \frac{\hat{W}^2_{\{3,4,5\}}}{\hat{W}^2_{\{1,2,3\}}}.$$
2. Degrade the S/N of SN 2001el in multiple steps with the addition of Poisson noise. Compute $\sigma^2_{\{1,2,3\}}$ and $\sigma^2_{\{3,4,5\}}$ at each step.
3. Extract γ_{31} by assuming a linear relationship between $\sigma^2_{\{1,2,3\}}$ and $\sigma^2_{\{3,4,5\}}$ (see middle panel of Figure 4).
$$\sigma^2_{\{3,4,5\}} = \beta + \gamma_{31} * \sigma^2_{\{1,2,3\}},$$
where $\sigma_{\{l\}}$ is defined in Equation (3).
4. Repeat each of the above steps over all regions of interest to extract a mean value for γ_{31}. Equivalently, use the values for γ_{31} by consulting Table 2.
5. Using Equation (4), compute ρ_{31} values for each SN having typical S/N values.
6. Compute the correction factor Π_{31} using this value of ρ_{31} and the value of γ_{31} computed for SN 2001el
$$\Pi_{31} = \sqrt{1 - \gamma_{31}\rho^2_{31}}.$$
7. The spectral index of any SNe feature can be corrected for bias by dividing the uncorrected value by Π_{31} as in Equation (3).
$$X_{\rm corr} = \frac{X}{\Pi_{31}}.$$
8. The error bars are determined from the same set of simulations. With σ_X defined as in Equation (6) construct the relationship
$$\log_{10}(\sigma_X) = \eta + \psi \log_{10}(\rho_{31}),$$
where all quantities refer to a SN with a large S/N (e.g., SN 2001el). Equivalently, use the values for η and ψ from Table 3.
9. With these values η and ψ compute the variance in the spectral index for a SN with a typical value of S/N as
$$\sigma_X = 10^{\eta}\rho^{\psi}_{31}.$$

4. APPLICATIONS TO TYPE IA SUPERNOVAE

Spectral indices lend themselves to a quantitative analysis of the temporal and magnitude evolution of the spectral lines. Nugent et al. (1995) measured the *ratio* of the depths of the Si II 6150 Å and 5750 Å features and established correlations with Δm_{15}. Other studies of these and other spectral features have adopted slightly more elaborate procedures based on equivalent (Hachinger et al. 2006) and pseudo-EWs (Folatelli 2004; Garavini et al. 2007a; Altavilla et al. 2009; Branch et al. 2009) to study these and other absorption features. Recently, Stanishev et al. (2007) and Arsenijevic et al. (2008) have used wavelets coupled with the pseudo-EW technique to study a Si II absorption feature. Emission features have received less attention and usually involve a distinct procedure from the absorption features (Nugent et al. 1995; Bongard et al. 2006). Recently, Bailey et al. (2009) described a variance of the above methods wherein absorption and emission features in a training set of spectra are studied to extract the optimal flux ratio to Δm_{15} correlation. This ratio is then applied to correct the magnitudes of other SNe within a validation set.

The wavelet technique developed here differs in several important respects from those described in the preceding paragraph. Our methodology is premised on the existence of one

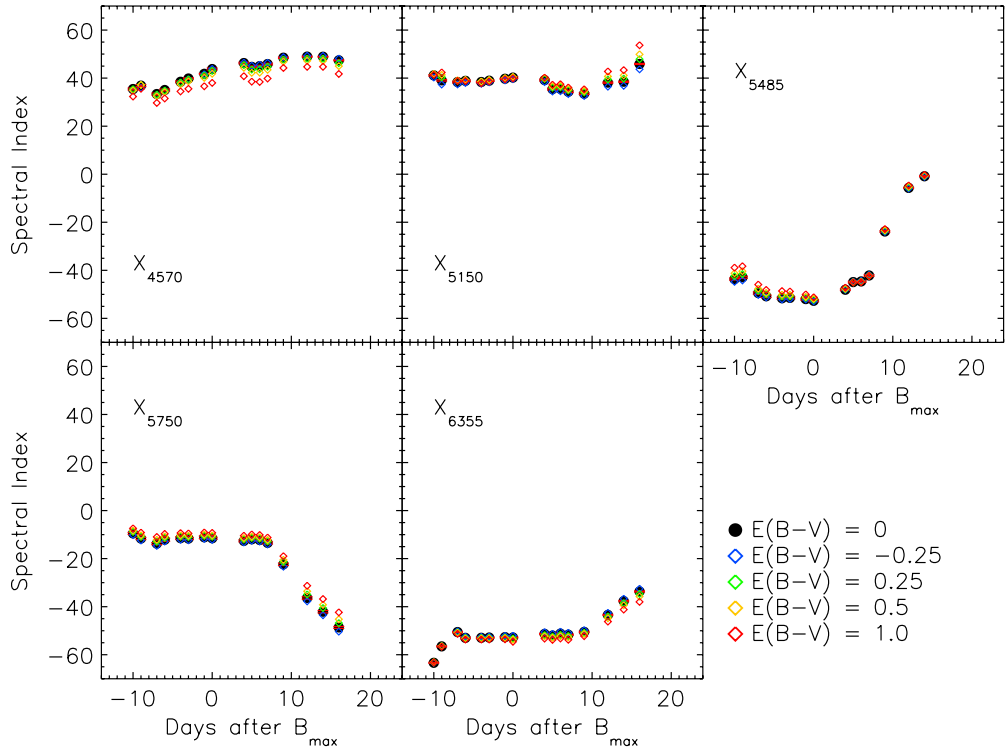

Figure 14. Same as Figure 7, but with the spectral indices recomputed separately for each of the 4 $E(B-V)$ values.
(A color version of this figure is available in the online journal.)

(or more) very high S/N spectra. Spectral line strengths are first extracted for this high S/N spectrum from a combination of intermediate wavelet scales. Excluding the lowest and highest reduces the effects of noise and the continuum, respectively. Working with wavelets from a high S/N spectrum allows corrections to be made to lower S/N spectra. Perhaps the most salient difference is that performing our analysis entirely in wavelet space permits us to avoid definition of the continuum (the mean of the wavelet scales is zero and integration is performed from one zero on the leading to the next zero on the trailing edge of a feature). Consequently, we are able to work directly with line strengths of the features themselves, not their ratios. Finally, this technique permits absorption and emission lines to be treated democratically. It is our expectation that the wavelet method gives to a more robust measure of line strength. In Sections 4.2 and 4.3, we apply this technique to data described in the subsequent section.

4.1. Data Sample

The SNe included in this study are given in Table 4. A large number of low-z spectra ($z < 0.1$) were collected from libraries that are publicly available, such as the SUSPECT SN Database[3] and the Center for Astrophysics SN Archive,[4] as well as other SNe that are available in the literature. The spectra are corrected by the host galaxy redshift but no dust extinction correction is applied. The original wavelength coverages, step sizes, and S/Ns of these spectra are vastly different. In our analysis, all the spectra are first rebinned to 5 Å sampling step for convenience. After wavelet decomposition was performed the spectra were checked for edge effects that would distort calculations, the affected spectra were removed.

[3] http://bruford.nhn.ou.edu/suspect/index1.html
[4] http://www.cfa.harvard.edu/supernova/SNarchive.html

4.2. X versus the Epochs

The evolution of spectral features in Type Ia SNe has been a topic of much study but due to the limitations of the pseudo-EW method and small sample sizes it has been mainly a qualitative study (for some more recent examples, see Branch et al. 2005; Garavini et al. 2007b; Pastorello et al. 2007; Quimby et al. 2007; Matheson et al. 2008; Wang et al. 2008). However, some Mg II, Fe II, and Ca II features have been studied quantitatively by Folatelli (2004) and Garavini et al. (2007a) using the pseudo-equivalent method. It is the hope of the authors that the wavelet spectral indexes described here will facilitate more quantitative studies of SNe Ia spectra.

An example of the time evolution of X indices is shown in Figure 7 for SN 2005cf—a normal Type Ia SN with $\Delta m_{15} = 1.16$. For a spectroscopically normal SN like SN 2005cf, X_{6150} and X_{5750} exhibit little evolution in line strength for roughly ±8 days around maximum. These two spectral indexes are associated at this epoch with the Si II 5972 and 6355 lines. After 8 days past maximum X_{5750} becomes stronger and X_{6150} weakens. Similarly, around 8 days past maximum X_{5485}, associated at maximum with the S II 5433/5459 Å "w" feature, begins to weaken until it is completely obscured by 18 days past maximum. The emission features at 4750 and 5150 Å for this same SN, by contrast, show comparatively little time evolution. These two emission features can be associated with P-Cygni profiles of Mg II and Si II, but are highly blended making identification difficult (Wang et al. 2006a).

Analysis of the time evolution is complicated by occasional large gaps between epochs and the need to occasionally track spectral features manually due to the decreasing velocity of the expanding photosphere. Consequently, a full analysis of the temporal evolution of the remaining SNe in Table 4 will be analyzed in a separate paper.

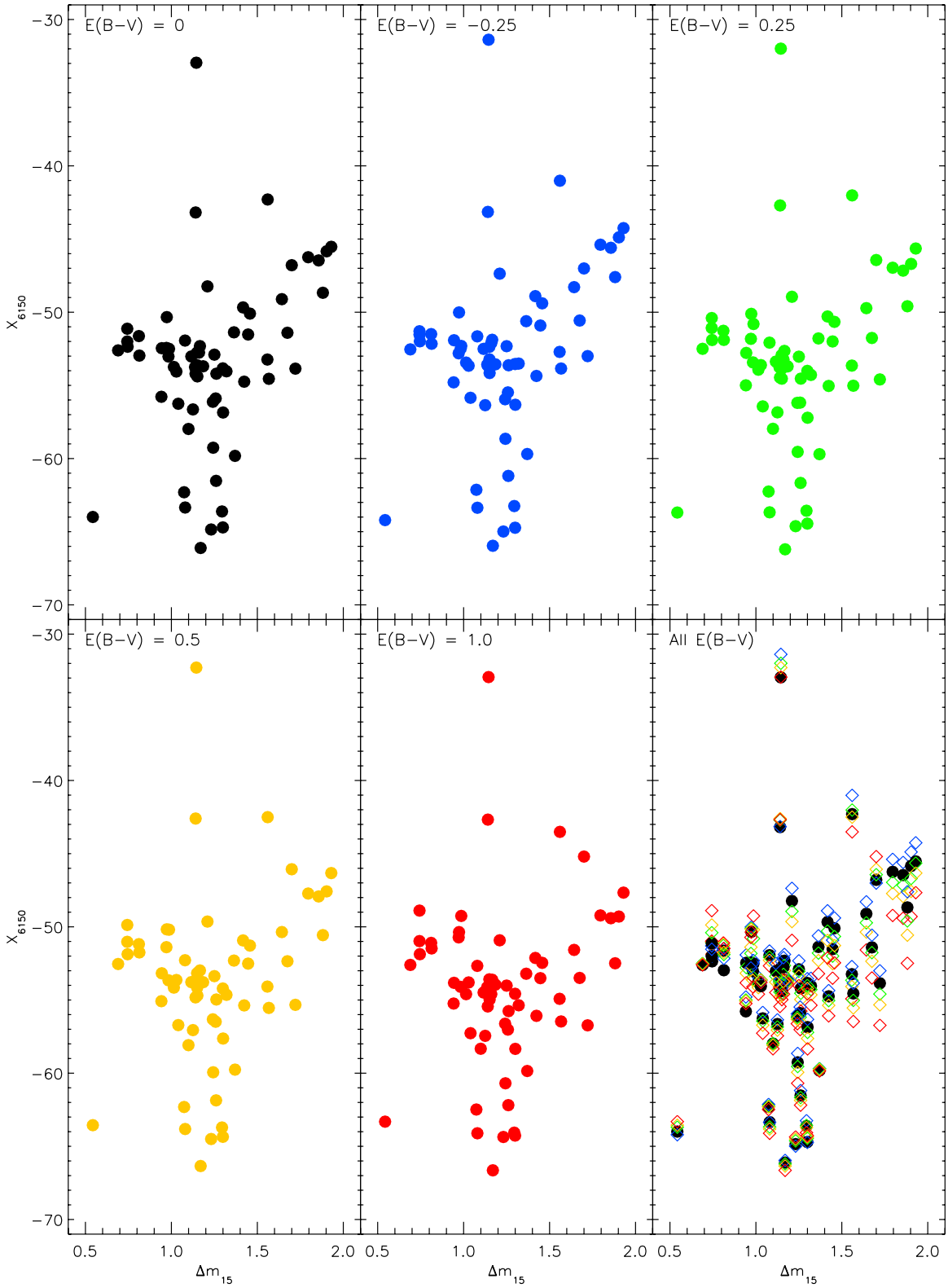

Figure 15. Same as Figure 8, but with the addition of four panels each displaying the spectral indices for four values of $E(B-V)$. The lower right panel overlays data from the first five panels.

(A color version of this figure is available in the online journal.)

4.3. X versus Δm_{15}

Figures 8–12 show the correlations between X and Δm_{15} for the five spectral features adopted for our study. The line strengths in these figures are those computed at maximum light. In instances where no spectrum at maximum light exists a simple quadratic fit was made of all spectra within 8 days of maximum (for features that are not a smoothly varying the fit

was restricted to within 5 days of maximum). The fits were checked for consistency and for SNe with only two spectra closely sampled in time, a mean was taken to avoid aberrant behavior in the fit. Any SN having only a single spectrum within the specified time range was removed, unless that spectrum was taken at maximum.

4.3.1. X_{6150}

It has been shown previously that the strength of the Si II 6355 Å line is not tightly correlated with the intrinsic brightness (Hachinger et al. 2006). The spectral index associated with this feature is X_{6150} and Figure 8 confirms this observation in the main. However, the X_{6150} indices do show a modest trend of weaker spectral strength for dimmer SNe and SNe with Δm_{15} greater than 1.0 show large variations of the index strength. Its merits mention that the several of these SNe (e.g., SN 1997br, SN 2001ay, SN 2002cx, and SN 2005hk) are deviant with respect to the majority of the sample. It has been noted that these are all peculiar SNe and it has been speculated that SN 1997br, SN 2002cx, and SN 2005hk may form a group distinct from most typical Type Ia SNe (Li et al. 1999, 2003; Branch et al. 2004, 2006, 2009; Howell & Nugent 2004; Jha et al. 2006; Phillips et al. 2007; Sahu et al. 2008).

4.3.2. X_{5750}

At maximum the X_{5750} index is a measure of the strength of the Si II absorption at 5972 Å. It has previously been shown that the ratio of the strength of this feature and that of the Si II 6355 Å line are well correlated with Δm_{15} (Nugent et al. 1995; Hachinger et al. 2006, 2008). Using this correlation, a determination of the supernova's maximum luminosity may be determined on the basis of a single spectra (Riess et al. 1998). These same two features have also been used to define Ia SNe subgroups (Benetti et al. 2005; Branch et al. 2006, 2009).

Figure 9 shows the correlations with Δm_{15}. The X indexes for this line correlate tightly with Δm_{15} even without having been divided by the strength of the Si II 6355 Å line (X_{6150} at maximum). Note however, that the X index for this feature is normalized by the total variance of the wavelength scales from wavelength region between 5500 Å and 6500 Å—the variations due to Si II 6355 Å line are partially included in the definition of this X index. The correlation between X and Δm_{15} is well described by a linear relation. There has been some discussion as to what physical process causes this correlation (see Garnavich et al. 2004; Branch et al. 2006; Bongard et al. 2008; Hachinger et al. 2008 for some examples). We wish to emphasize that the X index of this feature measures the total strength of this feature and does not distinguish the physical origins of the feature.

4.3.3. X_{5485}

The "w" shaped spectral feature S II 5433/5459 Å is another important line that defines a Type Ia SN similar to the Si II 6355 lines (Bongard et al. 2006; Hachinger et al. 2006). The X_{5485} index is a measurement of this feature at maximum. Figure 10 suggests that the strength of this feature too may depend on Δm_{15}, though the correlation is much weaker than that for X_{5750} (see e.g., Hachinger et al. 2008). The deviant SNe are SN 1991T, SN 2001ay, SN 2005hk, SN 2006X, SN 2001V, and SN 2002cx. SN 1997br has a similar spectral evolution to that of SN 1991T, but it has not been shown since it has only one spectrum within 5 days of maximum. However, the X value (−30) for SN 1997br at 4 days before maximum is consistent with the X value for SN 1991T. Other 1991T-like SNe (SN 1998es, SN 1999aa, SN 1999dq, SN 2000cx) have more typical values but they still are on the upper edge of the distribution. There is apparently some diversity among slow declining SNe.

The S II line is generally much stronger than the Si II 5972 line and is thus much easier to measure. There is also much more evolution within this feature, consequently Figure 10 is restricted to spectra taken within 5 days of maximum.

4.3.4. X_{5150}

The X_{5150} values decrease notably with Δm_{15} for the most sub-luminous SNe in Figure 11. However, there is much more scatter among the normal and slow-declining SNe. Figure 11 shows X_{5150} at maximum, and at this epoch this spectral index is associated at least in part with the P-Cygni profile of Si II at 5041 Å. From this figure, it is not possible to assert the efficacy of the emission feature at 5150 Å as an indicator of decline rate.

4.3.5. X_{4570}

This feature is partly associated with the Mg II feature at 4471 Å at maximum. As with the previous figure, Figure 12 shows what appears to be weak dependence on Δm_{15} with the 4570 Å emission peak. And as with Figures 9 and 10, the more deviant SNe appear on the outer edges of the distribution. This tendency is somewhat stronger than that found for the 5150 Å feature and is in the opposite direction: the X value for 4570 Å is increasing with increasing Δm_{15}.

There is wide variation in early time evolution to this feature, consequently the data comprising Figure 12 are restricted to spectra taken within 5 days of maximum. Similar to the 5150 Å feature, the utility of the 4750 Å feature in specifying decline rate is uncertain.

4.3.6. Ratio Between the Emission Features at 4570 Å and 5150 Å

The suggestion of a correlation between Δm_{15} and the ratio of these two features appears in Figure 13, though it is also weak, particularly for the fast decliners. It appears that the 4570 Å feature has a stronger effect on this ratio than the 5150 Å feature.

Due to the restriction on the 4570 Å feature, the same restriction to spectra within 5 days of maximum is applied to Figure 13. This ratio may be a useful parameter for the slower decliners but not for fast decliners.

4.4. Extinction

To explore the impact of reddening on the spectral indices, each spectrum in the SN sample in Table 4 was reddened. Four values for $E(B-V)$ were chosen: −0.25, 0.25, 0.5, and 1.0. An identical procedure to that described in Section 3 was applied to these reddened spectra and spectral indexes were recalculated.

Figures 14 and 15 are similar to Figures 7 and 8, but now include the effects of various values of $E(B-V)$. Figures 14 and 15 together demonstrate that reddening has only a minor effect on spectral indices and is, in any event, an effect that can be corrected.

5. CONCLUSIONS

Efforts to correlate the intrinsic brightness of Type Ia SNe with spectral line ratios or other methods related to feature strength are considerably complicated by line blending and

noise. We introduce a comparatively new technique to astronomical image processing based on an *à trous* wavelet decomposition and use it to extract spectral strengths of Type Ia SNe. In a straightforward manner, repeated application of the *à trous* generates successively smoother scales. The lowest scale can be identified with noise; a smooth residual results from truncating the algorithm at the highest scale. The intermediate scales are those that can be identified with spectral features and combining several of these intermediate scales provides a robust measure of spectral strength without having to wrestle with integration limits or a definition of the continuum. Monte Carlo methods in conjunction with a very high S/N Type Ia SN spectrum allows for correction of the spectral indices of SNe with lower S/N, even those whose S/N approach 1. These same methods readily permit error bars to be assigned to the spectral indices. The result is a definition of spectral line strength that is applied in this paper to the temporal evolution of spectral line strengths and the correlation of important spectral features with Δm_{15}. These indices are also shown to be largely impervious to reddening. A more robust spectral line strength like that developed here is likely to advance the identification or study of Type Ia subtypes or permit the construction of Type Ia templates with stretches that differ from unity. The latter effort, in particular, is directly related to our ongoing work on photometric redshift estimation relevant to the next generation of ground- and spaced-based survey telescopes.

REFERENCES

Altavilla, G., et al. 2007, A&A, 475, 585
Altavilla, G., et al. 2009, ApJ, 695, 135
Anupama, G. C. 1997, AJ, 114, 2054
Anupama, G. C., Sahu, D. K., & Jose, J. 2005, A&A, 429, 667
Arsenijevic, V., Fabbro, S., Mourão, A. M., & Rica da Silva, A. J. 2008, A&A, 492, 535
Bailey, S., et al. 2009, A&A, 500, L17
Barbon, R., Benetti, S., Rosino, L., Cappellaro, E., & Turatto, M. 1990, A&A, 237, 79
Barbon, R., Rosino, L., & Iijima, T. 1989, A&A, 220, 83
Benetti, S., et al. 2004, MNRAS, 348, 261
Benetti, S., et al. 2005, ApJ, 623, 1011
Bongard, S., Baron, E., Smadja, G., Branch, D., & Hauschildt, P. H. 2006, ApJ, 647, 513
Bongard, S., Baron, E., Smadja, G., Branch, D., & Hauschildt, P. H. 2008, ApJ, 687, 456
Branch, D., Baron, E., Hall, N., Melakayil, M., & Parrent, J. 2005, PASP, 117, 545
Branch, D., Baron, E., Thomas, R. C., Kasen, D., Li, W., & Filippenko, A. V. 2004, PASP, 116, 903
Branch, D., Dang, L. C., & Baron, E. 2009, PASP, 121, 238
Branch, D., Lacy, C. H., McCall, M. L., Sutherland, P. G., Uomoto, A., Wheeler, J. C., & Wills, B. J. 1983, ApJ, 270, 123
Branch, D., et al. 2003, AJ, 126, 1489
Branch, D., et al. 2006, PASP, 118, 560
Elias-Rosa, N., et al. 2006, MNRAS, 369, 1880
Filippenko, A. V., et al. 1992a, ApJ, 384, L15
Filippenko, A. V., et al. 1992b, AJ, 104, 1543
Folatelli, G. 2004, New Astron. Rev., 48, 623
Garavini, G., et al. 2004, AJ, 128, 387
Garavini, G., et al. 2005, AJ, 130, 2278
Garavini, G., et al. 2007, A&A, 470, 411
Garavini, G., et al. 2007, A&A, 471, 527
Garnavich, P. M., et al. 2004, ApJ, 613, 1120
Hachinger, S., Mazzali, P. A., & Benetti, S. 2006, MNRAS, 370, 299
Hachinger, S., Mazzali, P. A., Tanaka, M., Hillebrandt, W., & Benetti, S. 2008, MNRAS, 389, 1087
Hamuy, M., et al. 2002, AJ, 124, 417
Harris, G. L. H., Hesser, J. E., Massey, P., Peterson, C. J., & Yamanaka, J. M. 1983, PASP, 95, 607
Hernandez, M., et al. 2000, MNRAS, 319, 223
Hicken, M., Garnavich, P. M., Prieto, J. L., Blondin, S., DePoy, D. L., Kirshner, R. P., & Parrent, J. 2007, ApJ, 669, L17
Holtschneider, M, Kronland-Martinet, R., Morlet, J., & Tchamitchian, P. 1989, in Wavelets, Time–Frequency Methods and Phase Space, ed. J. M. Combes (Berlin: Springer), 289
Howell, A., & Nugent, P. 2004, in Cosmic Explosions in Three Dimensions: Asymmetries in Supernovae and Gamma-ray Bursts, ed. P. Hoflich, P. Kumar, & J. C. Wheeler (Cambridge: Cambridge Univ. Press), 151
Howell, D. A., et al. 2006, Nature, 443, 308
Jha, S., Branch, D., Chornock, R., Foley, R. J., Li, W., Swift, B. J., Casebeer, D., & Filippenko, A. V. 2006, AJ, 132, 189
Jha, S., et al. 1999, ApJS, 125, 73
Kirshner, R. P., et al. 1993, ApJ, 415, 589
Kotak, R., et al. 2005, A&A, 436, 1021
Krisciunas, K., et al. 2007, AJ, 133, 58
Leibundgut, B., Kirshner, R. P., Filippenko, A. V., Shields, J. C., Foltz, C. B., Phillips, M. M., & Sonneborn, G. 1991, ApJ, 371, L23
Leibundgut, B., et al. 1993, AJ, 105, 301
Li, W. D., et al. 1999, AJ, 117, 2709
Li, W., et al. 2001, PASP, 113, 1178
Li, W., et al. 2003, PASP, 115, 453
Matheson, T., et al. 2008, AJ, 135, 1598
Mazzali, P. A., Lucy, L. B., Danziger, I. J., Gouiffes, C., Cappellaro, E., & Turatto, M. 1993, A&A, 269, 423
Mazzali, P. A., Sauer, D. N., Pastorello, A., Benetti, S., & Hillebrandt, W. 2008, MNRAS, 386, 1897
Meikle, W. P. S., et al. 1996, MNRAS, 281, 263
Meikle, P., & Hernandez, M. 2000, Mem. Soc. Astron. Ital., 71, 299
Nugent, P., Phillips, M., Baron, E., Branch, D., & Hauschildt, P. 1995, ApJ, 455, L147
Patat, F., Benetti, S., Cappellaro, E., Danziger, I. J., della Valle, M., Mazzali, P. A., & Turatto, M. 1996, MNRAS, 278, 111
Pastorello, A., et al. 2007, MNRAS, 377, 1531
Perlmutter, S., et al. 1997, ApJ, 483, 565
Phillips, M. M., Wells, L. A., Suntzeff, N. B., Hamuy, M., Leibundgut, B., Kirshner, R. P., & Foltz, C. B. 1992, AJ, 103, 1632
Phillips, M. M., et al. 1987, PASP, 99, 592
Phillips, M. M., et al. 2007, PASP, 119, 360
Pignata, G., et al. 2008, MNRAS, 388, 971
Quimby, R., Höflich, P., Kannappan, S. J., Rykoff, E., Rujopakarn, W., Akerlof, C. W., Gerardy, C. L., & Wheeler, J. C. 2006, ApJ, 636, 400
Quimby, R., Höflich, P., & Wheeler, J. C. 2007, ApJ, 666, 1083
Riess, A. G., Nugent, P., Filippenko, A. V., Kirshner, R. P., & Perlmutter, S. 1998, ApJ, 504, 935
Ruiz-Lapuente, P., Cappellaro, E., Turatto, M., Gouiffes, C., Danziger, I. J., della Valle, M., & Lucy, L. B. 1992, ApJ, 387, L33
Sahu, D. K., et al. 2008, ApJ, 680, 580
Salvo, M. E., Cappellaro, E., Mazzali, P. A., Benetti, S., Danziger, I. J., Patat, F., & Turatto, M. 2001, MNRAS, 321, 254
Shensa, M. J. 1992, Proc. IEEE Trans. Signal Process., 40, 2464
Starck, J.-L., Murtagh, F., & Bijaoui, A. 1995, in ASP Conf. Ser. 77, Astronomical Data Analysis Software and Systems IV, ed. R. A. Shaw, H. E. Payne, & J. J. E. Hayes (San Francisco, CA: ASP), 279
Starck, J.-L., Siebenmorgen, R., & Gredel, R. 1997, ApJ, 482, 1011
Stanishev, V., et al. 2007, A&A, 469, 645
Strolger, L.-G., et al. 2002, AJ, 124, 2905
Taubenberger, S., et al. 2008, MNRAS, 385, 75
Turatto, M., Benetti, S., Cappellaro, E., Danziger, I. J., Della Valle, M., Gouiffes, C., Mazzali, P. A., & Patat, F. 1996, MNRAS, 283, 1
Valentini, G., et al. 2003, ApJ, 595, 779
Wang, L., Baade, D., Höflich, P., Wheeler, J. C., Kawabata, K., Khokhlov, A., Nomoto, K., & Patat, F. 2006a, ApJ, 653, 490
Wang, L., Strovink, M., Conley, A., Goldhaber, G., Kowalski, M., Perlmutter, S., & Siegrist, J. 2006b, ApJ, 641, 50
Wang, L., Wheeler, J. C., & Hoeflich, P. 1997, ApJ, 476, L27
Wang, L., et al. 2003, ApJ, 591, 1110
Wang, X., et al. 2008, ApJ, 675, 626
Wells, L. A., et al. 1994, AJ, 108, 2233